Theoretical model analysis of deuteron-induced reactions and development of an integrated code system for cross section evaluation

中山, 梓介

https://doi.org/10.15017/1500764

出版情報：九州大学, 2014, 博士（工学）, 課程博士
バージョン：

Theoretical model analysis of deuteron-induced reactions and development of an integrated code system for cross section evaluation

Shinsuke Nakayama

Department of Advanced Energy Engineering Science

Interdisciplinary Graduate School of Engineering Sciences

Kyushu University

February 2015

Contents

Chapter 1

Introduction

1.1 Deuteron accelerator neutron sources

In recent years, intensive neutron sources using deuteron accelerator have been proposed for various applications. In these facilities, the (*d*,*xn*) reaction on light nuclei (Li, Be, C, etc.) is considered as a promising reaction to generate intensive neutron beams. Fig.1.1 shows experimental thick target neutron yields from (*p*,*xn*) and (*d*,*xn*) reactions on ^{9}Be [1.1, 1.2]. This figure shows some advantages of a (*d*,*xn*) neutron source over a widely-used (*p*,*xn*) neutron source. First, the amount of generated neutrons is large. Second, the neutron spectrum has a broad energy peak around half the deuteron incident energy. This means that the most probable neutron energy can be changed by adjusting incident deuteron energy. In addition, the (*d*,*xn*) reaction has strongly forward-peaked angular distribution, which is an additional advantage from the point of view of shielding.

From these favorable features, intensive neutron sources using deuteron accelerator have been proposed for various applications involved with not only international scientific projects such as International Fusion Materials Irradiation Facility (IFMIF) [1.3] and Neutron For Science (NFS) in SPIRAL2 [1.4], but also medical applications such as Boron Neutron Capture Therapy (BNCT) [1.5] and production of radioisotopes for medical use [1.6, 1.7].

In the above various applications, we pay particular attention to the generation of medical isotopes ^{64}Cu ($T_{1/2}$ = 12.7 h) with neutrons generated by C(*d*,*xn*) reactions [1.7]. ^{64}Cu is one of radionuclide for positron emission tomography (PET) and PET is used for diagnosis of tumor cell and the dynamics of a medicine in living body. To produce ^{64}Cu, it is expected that the ^{64}Zn(*n*,*p*)^{64}Cu reaction with neutrons below 10 MeV will be effective.

This is because Fig. 1.2 indicates that by-products via the other reactions are expected to be suppressed in this energy range. The selectivity of the most probable neutron energy for (*d*,*xn*) neutron sources is useful in the case where a certain neutron energy range is required like this case.

1.2 Requirement for deuteron nuclear data

As mentioned above, light nuclei (Li, Be, C, etc.) is considered as a deuteron target material in deuteron accelerator neutron sources. In addition, deuteron accelerator components consist of various structure materials including Fe, Cr, Ni, etc. as well as target materials. Thus, accurate nuclear database of deuteron-induced reactions over wide ranges of target mass number and incident deuteron energy are indispensable for engineering design of deuteron accelerator neutron sources.

Currently available deuteron nuclear data file is TENDL (TALYS-based evaluated nuclear data library) [1.9] which has been developed by compiling the output of TALYS code [1.10]. Fig.1.3 shows the comparison of double-differential cross sections calculated with TALYS code and experimental data [1.11] for ^{58}Ni (*d*,*xp*) at 100MeV. The calculation result underestimates considerably a characteristic broad peak observed around half the deuteron incident energy in experimental data. In addition, as shown in Fig. 1.4, calculation results of TALYS code underestimate the experimental data [1.12, 1.13] of production cross section of radioactive nucleus ^{46}Sc ($T_{1/2}$ = 83.79 day) from ^{45}Sc(*d*,*p*) reactions. From these two figures, it can be said that the present TALYS code is not necessarily adequate for calculation of deuteron-induced reactions. Thus, new comprehensive and accurate nuclear data of deuteron-induced reactions are required for the development and engineering design of deuteron accelerator neutron sources.

Figure 1.5 shows a flowchart of development of deuteron nuclear data and its applications. Since the number of cross section data to be stored in deuteron nuclear data is very large, it is impossible to create it

based on experimental data alone. Therefore, in order to develop the new deuteron nuclear data, it is necessary to develop an integrated code system based on theoretical models for deuteron-induced reactions. In addition, careful validation of applicability of the code system over the wide ranges of target mass number and incident deuteron energies should be made. If the calculation results fail to reproduce experimental data, one needs to adjust input parameters used in the calculations or refine the calculation models. After these processes, "evaluated" values of cross sections are stored in deuteron nuclear data. Deuteron nuclear data is compiled in the form of ENDF (Evaluated Nuclear Data File) format and then processed to ACE (A Compact ENDF) format by NJOY code [1.14]. ACE is a format of nuclear data used in Monte Carlo code such as PHITS (Particle and Heavy Ion Transport Code System) [1.15]. In this way, deuteron nuclear data will be used in the engineering design and development of deuteron accelerator neutron sources for various applications.

1.3 Deuteron induced reactions

Deuteron is a very loosely bound system of a proton and a neutron and its binding energy is 2.225 MeV. As shown in Fig.1.6, therefore, characteristic reaction processes on deuteron-induced reaction such as elastic breakup and stripping reaction are likely to occur, and these reactions are expected to make a large contribution to various deuteron-induced reaction cross sections. Thus, it is important to choose theoretical models to describe adequately both the breakup and stripping processes.

Under the circumstance, Ye et al. proposed a theoretical model calculation method in order to describe nucleon emissions from deuteron-induced reactions quantitatively [1.16, 1.17]. In the calculation method, the Continuum Discretized Coupled-Channels method (CDCC) [1.18] and the Glauber model [1.19] were used to calculate elastic breakup and stripping reactions, respectively. As a result of analysis at incident

energies up to 100MeV, it was shown that the calculation results reproduce broad peak observed around half the incident deuteron energy in experimental data fairly well at small angles.

However, in their method, the phenomenological moving-source (MS) model was used to estimate statistical decay components, *i.e.*, pre-equilibrium and evaporation components. The MS model has low predictive power because it needs some parameters determined by fitting the experimental data. This means that the MS models is not necessarily adequate for calculation toward development of nuclear data. In addition, the Glauber model cannot treat the stripping reaction to bound states in the residual nucleus properly and relative contribution of this component gets larger at incident energies below 50MeV. Since this incident energy range is important for various application fields, we should consider the stripping reaction to bound states properly for development of deuteron nuclear data.

1.4 The purpose of this work

As shown in Fig. 1.5, theoretical cross section calculation plays an important role in development of deuteron nuclear data. However, so far there has been no code system which can be used for development of comprehensive and accurate deuteron nuclear data. Taking into consideration these circumstances, the purposes of this work are as follows:

- To develop an integrated code system dedicated for deuteron-induced reactions
- To validate the code system through analysis of available experimental cross section data

In Chapter 2, brief explanations about the code system we developed and the theoretical models used in it are provided.

In Chapter 3, systematic investigation of spectroscopic factors

(SFs) which are necessary to determine the absolute values of DWBA calculations are performed. SFs for the (d,p) reactions on ^{12}C, ^{27}Al, ^{40}Ca, and ^{58}Ni for incident deuteron energies up to 100 MeV are extracted systematically by fitting theoretical DWBA calculations to the exiting experimental data.

In Chapter 4, the code system is applied to analysis of double-differential cross sections (DDXs) for the (d,xp) reactions on ^{12}C, ^{27}Al, and ^{58}Ni at 25.5, 56, and 100MeV.

In Chapter 5, the code system is also applied to analysis of production cross sections of radioactive nuclei from the (d,p) reactions on ^{27}Al and ^{45}Sc at incident energies from threshold to 50 MeV.

Finally, Chapter 6 gives a summary of this work, and perspectives of the future works are described.

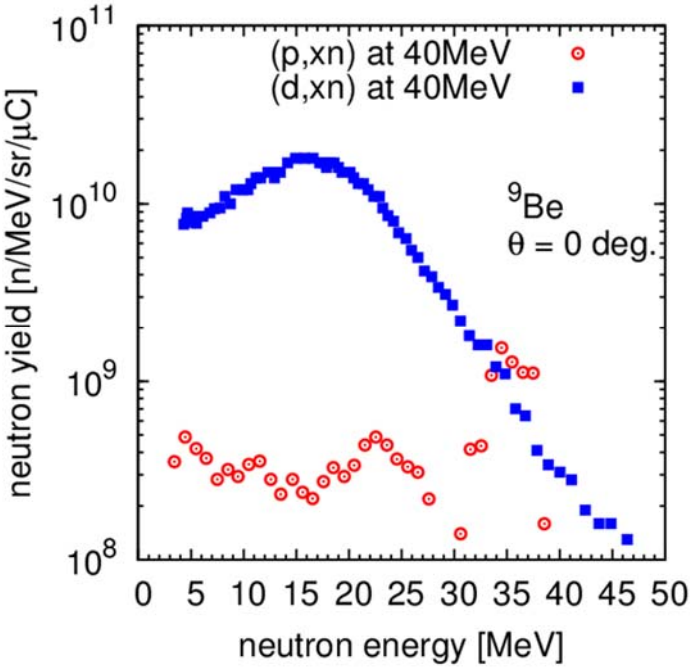

Fig. 1.1 Thick target neutron yields from (*p*,*xn*) and (*d*,*xn*) reactions on ^{9}Be at 40 MeV.

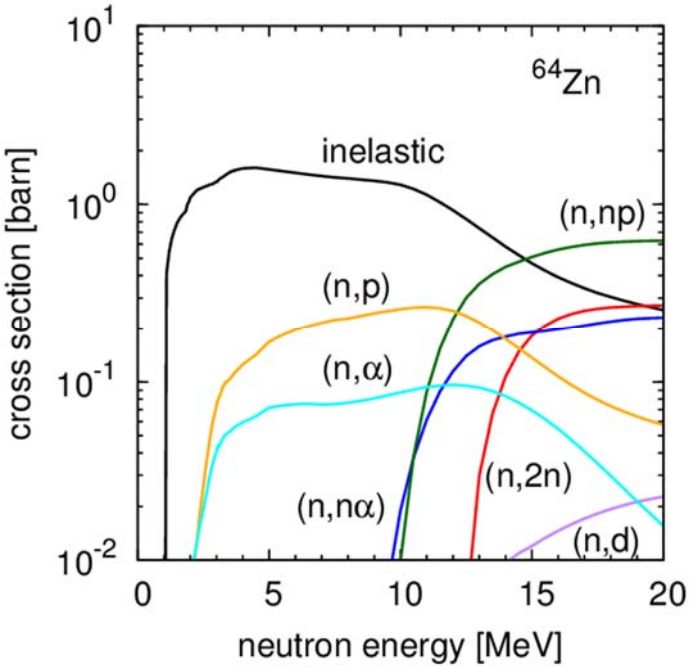

Fig. 1.2 Neutron cross sections for ^{64}Zn taken from JENDL-4.0 [1.8].

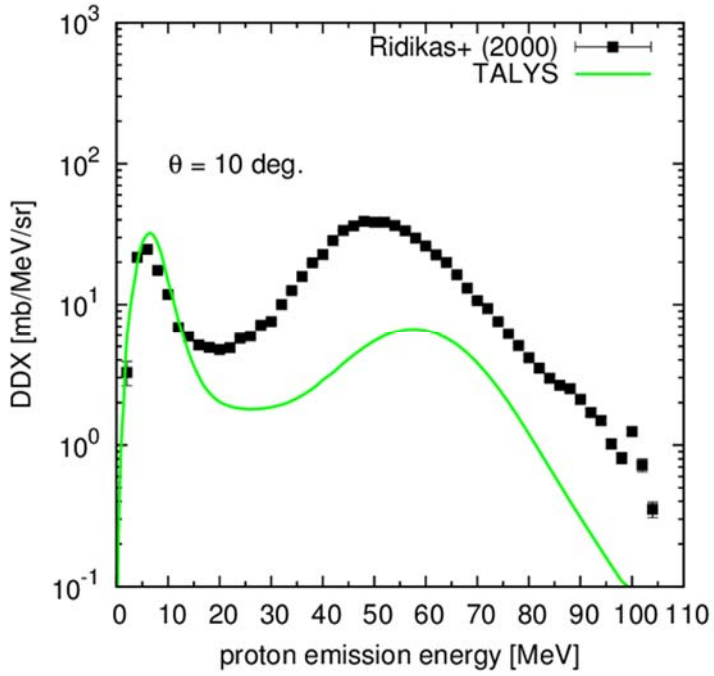

Fig. 1.3 Comparison of calculation with TALYS code
and experimental data for double-differential cross sections
for (*d,xp*) reaction on ^{58}Ni at 100MeV.

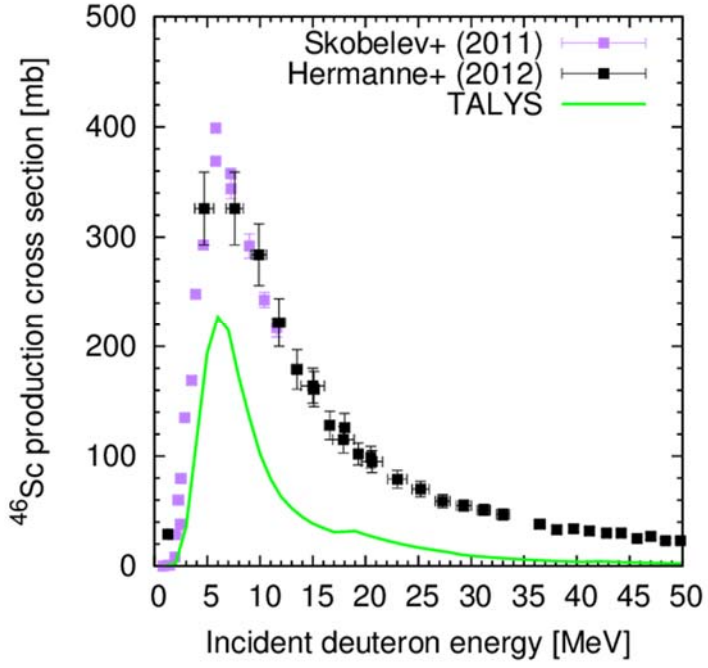

Fig. 1.4 Same as Fig. 1.3 but for
production cross section of ^{46}Sc from ^{45}Sc(*d,p*) reactions.

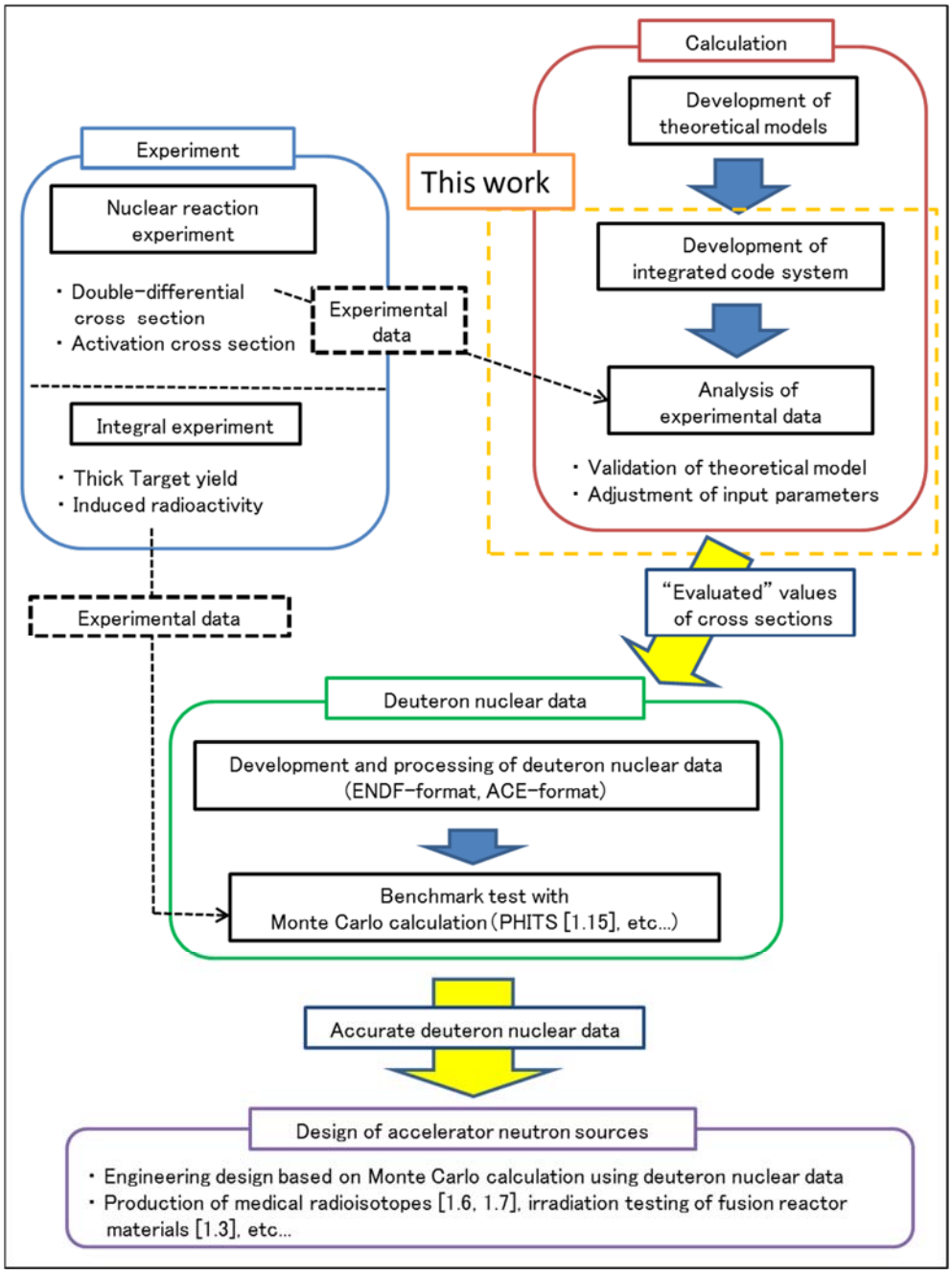

Fig. 1.5 Flowchart of development of deuteron nuclear data

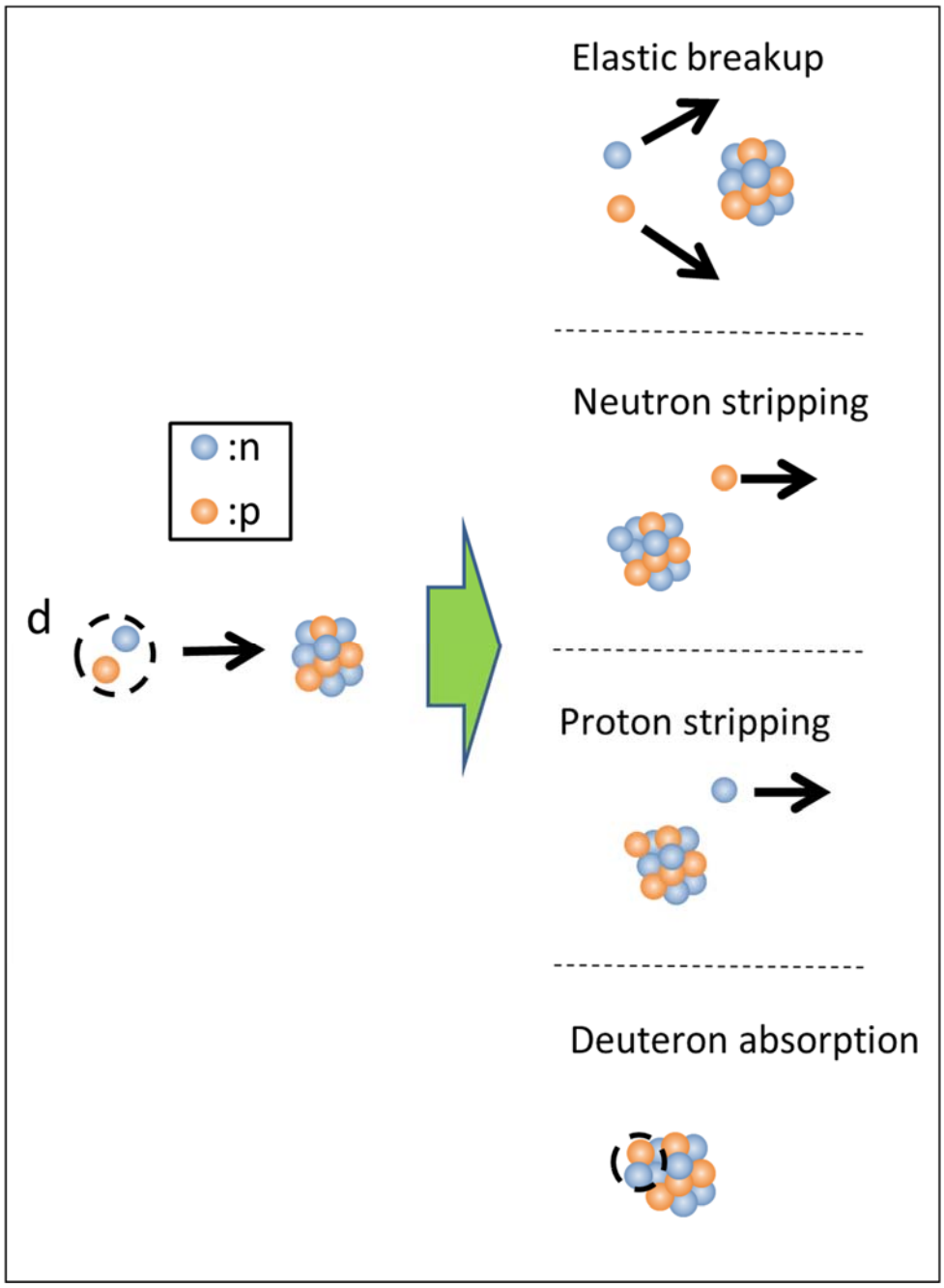

Fig. 1.6 Schematic view of various deuteron-induced reactions.

Bibliography

[1.1] M. J. Saltmarsh, C. A. Ludemann, C. B. Fulmer, R. C. Styles, "Characteristics of an intense neutron source based on the d+Be reaction", Nucl. Instr. Meth. **145**, 81-90 (1977).

[1.2] Y. Uwamino, T. Okubo, A. Torii, T. Nakamura, "Semi-monoenergetic neutron field for activation experiments up to 40 MeV", Nucl. Instr. Meth. A **271**, 546-552 (1988).

[1.3] A. Moeslang, V. Heinzel, H. Matsui, M. Sugimoto, "The IFMIF test facilities design", Fusion Eng. Des. **81**, 863-871 (2006).

[1.4] M. Fadil, B. Rannou, the SPIRAL2 project team, "About the production rates the activation of the uranium carbide target for SPIRAL 2", Nucl. Instr. Meth. B **266**, 4318-4321 (2008).

[1.5] S. Agosteo, G. Curzio, F. d'Errico, R. Nath, R. Tinti, "Characterization of an accelerator-based neutron source for BNCT versus beam energy", Nucl. Instr. Meth. A **476**, 106-112 (2002).

[1.6] Y. Nagai, K. Hashimoto, Y. Hatsukawa, H. Saeki, S. Motoishi, N. Sato, M. Kawabata, H. Harada, T. Kin, K. Tsukada, T. Sato, F. Minato, O. Iwamoto, N. Iwamoto, Y. Seki, K. Yokoyama, T. Shiina, A. Ohta, N. Takeuchi, Y. Kawauchi, N. Sato, H. Yamabayashi, Y. Adachi, Y. Kikuchi, T. Mitsumoto, T. Igarashi, "Generation of Radioisotopes with Accelerator Neutrons by Deuterons", J. Phys. Soc. Jpn. **82**, 064201 (2013).

[1.7] T. Kin, Y. Nagai, N. Iwamoto, F. Minato, O. Iwamoto, Y. Hatsukawa, M. Segawa, H. Harada, C. Konno, K. Ochiai, K. Takakura, "New Production Routes for Medical Isotopes ^{64}Cu and ^{67}Cu Using Accelerator Neutrons", J. Phys. Soc. Jpn. **82**, 034201 (2013).

[1.8] K. Shibata, O. Iwamoto, T. Nakagawa, N. Iwamoto, A. Ichihara, S.

Kunieda, S. Chiba, K. Furutaka, N. Otuka, T. Ohsawa, T. Murata, H. Matsunobu, A. Zukeran, S. Kamada, J. Katakura, "JENDL-4.0: A new library for nuclear science and engineering", J. Nucl. Sci. Technol. **48**, 1-30 (2011).

[1.9] A.J. Koning and D. Rochman, "Modern nuclear data evaluation with the TALYS code system", Nucl. Data Sheets **113**, 2841-2934 (2012).

[1.10] A.J. Koning, S. Hilaire and M.C. Duijvestijn, "TALYS-1.0", Proc. the International Conference on Nuclear Data for Science and Technology, 211-214, Nice, France, 22-27 Apr (2007)

[1.11] D. Lidikas, W. Mittig, H. Savajols, P. Roussel-Chomaz, S. V. Fortsch, J. J. Lawrie, G. F. Steyn, "Inclusive proton production cross sections in (*d*,*xp*) reactions induced by 100 MeV deuterons", Phys. Rev. C **63**, 014610 (2000).

[1.12] A. Hermanne, R. Adam Rebeles, F. Tarkanyi, S. Takacs, M.P. Takacs, J. Csikai, A. Ignatyuk, "Cross sections of deuteron induced reactions on ^{45}Sc up to 50 MeV: Experiments and comparison with theoretical codes", Nucl. Inst. Meth. B **270**, 106-115 (2012).

[1.13] N.K. Skobelev, A.A. Kulko, V. Kroha, V. Burjan, Z. Hons, A.V. Daniel, N.A. Demekhina, R. Kalpakchieva, A. Kugler, J. Mrazek, Yu.E. Penionzhkevich, S. Piskor, E. Simeckova, E.I. Voskoboynik, "Excitation functions for the radionuclide ^{46}Sc produced in the irradiation of ^{45}Sc with Deuterons and ^{6}He, J. Phys. G Nucl. Part. Phys. **38** 035106 (2011).

[1.14] R. E. MacFarlane and D.W. Muir "The NJOY nuclear data processing system. Version91", LA-12740-M, Los Alamos National Laboratory (1994).

[1.15] T. Sato, K. Niita, N. Matsuda, S. Hashimoto, Y. Iwamoto, S. Noda, T. Ogawa, H. Iwase, H. Nakashima, T. Fukahori, K. Okumura, T. Kai, S. Chiba, T. Furuta and L. Sihver, "Particle and Heavy Ion Transport Code System PHITS, Version 2.52", J. Nucl. Sci.

Technol. **50**, 913-923 (2013).

[1.16] T. Ye, Y. Watanabe, K. Ogata, "Analysis of deuteron breakup reactions on ^{7}Li for energies up 100MeV", Phys. Rev. C **80**, 014604 (2011).

[1.17] T. Ye, S. Hashimoto, Y. Watanabe, K. Ogata, M. Yahiro, "Analysis of inclusive (*d*,*xp*) reactions on nuclei from ^{9}Be to ^{238}U at 100 MeV", Phys. Rev. C **84**, 054606 (2011).

[1.18] M. Yahiro, K. Ogata, T. Matsumoto, K. Minomo, "The continuum discretized coupled-channels method and its applications", Prog. Theor. Exp. Phys. **2012**, 01A206 (2012), and references therein.

[1.19] R. J. Glauber, in Lectures in Theoretical Physics (Interscience, New York, 1959), Vol. 1, p. 315.

Chapter 2

Theoretical models

The code system developed in the present work consists of several model codes to describe respective reaction mechanisms characteristic for deuteron-induced reactions. In this chapter, the structure of the code system and the theoretical models used in it are outlined.

2.1 Structure of the integrated code system

Figure 2.1 shows the structure of the integrated code system. Elastic breakup reaction is calculated with the codes based on the Continuum-Discretized Coupled-Channels method (CDCC) [2.1]. Stripping reactions to bound states in the residual nuclei are calculated using the DWUCK4 [2.2], which is the computational code based on conventional zero-range Distorted Wave Born Approximation (DWBA). In the DWBA calculation, spectroscopic factors (SFs) are necessary to determine the absolute value of calculations. With respect to SFs, detailed description is given in Chapter 3. Next, the computational code based on the Glauber model [2.3] is used to calculate the stripping reactions to continuum. Finally, statistical decay components from compound nuclei are calculated using the Hauser-Feshbach and exciton models implemented in the CCONE code [2.4] which was successfully applied to neutron nuclear data evaluation for JENDL-4.0 [2.5]. As described in Chapters 4 and 5, the CCONE results for three different compound nuclei are finally averaged by the formation fractions calculated with the Glauber model. In the following sections, the individual theoretical models are outlined.

2.2 CDCC method

The basic idea of CDCC [2.1] is to truncate and discretize the infinite number of breakup continuum states of the weekly bound projectile such as deuteron to finite number of discrete states with respect to its fragmentation and relative momentum (or excitation energy), and to introduce them to the coupled channel (CC) equations.

According to Ref. [2.6], in the case where proton is detected via the elastic breakup process, the triple differential cross section for elastic breakup in the laboratory system is expressed as

$$\frac{d^2\sigma_{EB}}{d\Omega_n^L d\Omega_p^L dE_p^L} = \frac{2\pi}{\hbar}\frac{\mu_i}{P_d}\left|T_{fi}\right|^2 \rho(E_p^L), \tag{2.1}$$

where $d\Omega_n^L$ and $d\Omega_p^L$ represent the emission direction of neutron and proton, respectively, E_p^L is the proton emission energy, μ_i is the reduced mass of the initial state, P_d is the momentum of the incident deuteron, T_{fi} is the transition matrix element, and $\rho(E_p^L)$ is the three-body phase space factor [2.7]. T_{fi} is given by Eq. (2.10) in Ref. [2.6].

The double differential cross section with respect to the proton emission energy and angle is obtained by integrating the Eq. (2.1) over neutron emission angle:

$$\frac{d^2\sigma_{EB}}{d\Omega_p^L dE_p^L} = \int \frac{d^2\sigma_{EB}}{d\Omega_n^L d\Omega_p^L dE_p^L} d\Omega_n^L . \tag{2.2}$$

2.3 DWBA

The DWBA has been quite widely used for the analysis of direct process such as (*d*,*p*) stripping reaction. In the present code system, DWBA calculations are performed with the DWUCK4 code [2.2]. In the

DWUCK4, it is assumed that the transfer process occurs in the only one step. Under this assumption, the angular differential cross section of (*d*,*p*) reaction are given as follows:

$$\frac{d\sigma_{(d,p)}}{d\Omega} = \frac{\mu_i \mu_f}{(2\pi\hbar)^2} \frac{k_p}{k_d} \left| T_{DWBA} \right|^2 , \tag{2.3}$$

where μ_i and μ_f are the reduced masses of initial and final state, respectively, k_p and k_d are the wave numbers of deuteron and proton, respectively, and T_{DWBA} is the transition matrix element of DWBA. T_{DWBA} is expressed by Eq. (2.4).

$$T_{DWBA} = \left\langle \chi_f^{(-)} \Phi_{nA} \left| V_{pn} \right| \Phi_d \chi_i^{(+)} \right\rangle \ , \tag{2.4}$$

where $\chi_i^{(+)}(\mathbf{r}_i)$ and $\chi_f^{(-)}(\mathbf{r}_f)$ are distorted waves between the deuteron and the target nucleus in the initial state and the proton and the residual nucleus in the final state, $\Phi_d(\mathbf{r}_{pn})$ is the wave function of deuteron, $\Phi_{nA}(\mathbf{r}_{nA})$ is the bound state wave function of neutron in the residual nucleus, and $V_{pn}(\mathbf{r}_{pn})$ is the residual interaction. The coordinate system in DWBA calculation is shown in Fig. 2.2.

In the DWUCK4, the zero-range approximation is used as follows:

$$V_{pn}(\mathbf{r}_{pn}) \Phi_d(\mathbf{r}_{pn}) = D_0 \delta(\mathbf{r}_{pn}) , \tag{2.5}$$

where D_0 is called zero-range constant. In the present work we introduce the finite-range correction to the zero-range approximation and the form factor is multiplied by the following function:

$$W_{FR}(r) = \left[1 + A(r) \right]^{-1} \tag{2.6}$$

and

$$A(r) = \frac{2}{\hbar^2} \frac{m_p m_n}{m_d} R^2 \left(E_p - V_p(r_p) + E_n - V_n(r_n) - E_d + V_d(r_d) \right). \tag{2.7}$$

where m_p, m_n, m_d and E_p, E_n, E_d and V_p, V_n, V_d are the masses, the energies, and the potentials of proton, neutron, and deuteron, respectively. R is called as finite range correction factor. In addition, we also use the correction for non-locality of optical potentials and the distorted waves are multiplied by the following coefficient:

$$W_{NL}(r_i) = \exp\left(\frac{\beta_i^2}{8} \frac{2m_i}{\hbar^2} V_i(r_i) \right), \tag{2.8}$$

where β_i is the non-locality parameter for particle i and defined for proton and deuteron.

2.4 Glauber model

In the present code system, the computational code based on the Glauber model [2.3] are used to calculate DDXs for stripping reactions to continuum and the cross section of deuteron absorption, proton stripping, and neutron stripping, respectively. The Glauber model is a semi-classical model using the eikonal and adiabatic approximations. In the Glauber model, the scattering matrix S is given by

$$S(b_d) = \exp\left(i\chi_d(b_d)\right), \tag{2.9}$$

and

$$\chi_d(b_d) = -\frac{1}{\hbar v} \int_{-\infty}^{+\infty} V_d(\sqrt{b_d^2 + z^2}) dz, \tag{2.10}$$

where χ_d is the eikonal phase shift, b_d is the impact parameter perpendicular to the deuteron incident direction along the z axis, v is the relative velocity between the deuteron and the target nucleus, and V_d is the deuteron potential. In this work, V_d is expressed by the sum of the proton potential V_p and the neutron potential V_n, and in this case $\chi_d(b_d)$ is the sum of the phase shift for proton $\chi_p(b_p)$ and that for neuteron $\chi_n(b_n)$ as follows:

$$\chi_d(b_d) = \chi_p(b_p) + \chi_n(b_n), \tag{2.11}$$

where b_p and b_n is the impact parameter of proton and neutron perpendicular to the z axis. The scattering matrices for proton and neutron are defined by

$$\begin{cases} S_p(b_p) = \exp\left(i\chi_p(b_p)\right) = \exp\left(-\dfrac{i}{\hbar v}\displaystyle\int_{-\infty}^{+\infty} V_p\left(\sqrt{b_p^2 + z^2}\right)dz\right) \\ S_n(b_n) = \exp\left(i\chi_n(b_n)\right) = \exp\left(-\dfrac{i}{\hbar v}\displaystyle\int_{-\infty}^{+\infty} V_n\left(\sqrt{b_n^2 + z^2}\right)dz\right) \end{cases}. \tag{2.12}$$

In this work, a phenomenological optical potentials (OPs) is used for V_p and V_n. Since the integral in Eq. (2.12) for the Coulomb part of the proton OPs diverge, the Coulomb eikonal phase shift is added to the $\chi_p(b_p)$ calculated using V_p without the Coulomb potential same as Ref. [2.8].

The differential cross section for the neutron stripping process is given in the center of mass of the p-n system by the following expression [2.9]:

$$\frac{d\sigma_{STR}}{dk_p^C} = \frac{1}{(2\pi)^3}\int d^2\mathbf{b}_n \left\{\left(1 - \left|S_n(b_n)\right|^2\right)\left(\int d^3\mathbf{r} e^{-i\mathbf{k}_p^C\cdot\mathbf{r}} S_p(b_p)\varphi_{00}(\mathbf{r})\right)^2\right\}, \tag{2.13}$$

where $\mathbf{r}$ is the relative coordinate between the proton and neutron in the deuteron, k_p^C is the proton-wave-number vector, and $\varphi_{00}(\mathbf{r})$ is the wave function of the deuteron ground state. The double differential cross section of neutron stripping reaction can be obtained by transforming the Eq. (2.13) to the laboratory system:

$$\frac{d^2\sigma_{Glauber}}{dEd\Omega} = \frac{m_p k_p^L}{\hbar^2}\frac{d\sigma_{STR}}{dk_p^C}. \tag{2.14}$$

Next, the total reaction cross section σ_{REA}, the proton stripping reaction cross section σ_{p-STR}, the neutron stripping reaction cross section

σ_{n-STR}, and the elastic breakup cross section σ_{EB} can be calculated as follows:

$$\sigma_{REA} = \int d^2\mathbf{b}_d \left(1 - \left| \int d^3\mathbf{r} \left|\varphi_{00}(\mathbf{r})\right|^2 S_p(b_p) S_n(b_n) \right|^2 \right), \tag{2.15}$$

$$\sigma_{p-STR} = \int d^2\mathbf{b}_d \int d^3\mathbf{r} \left|\varphi_{00}(\mathbf{r})\right|^2 \left|S_n(b_n)\right|^2 \left(1 - \left|S_p(b_p)\right|^2\right), \tag{2.16}$$

$$\sigma_{n-STR} = \int d^2\mathbf{b}_d \int d^3\mathbf{r} \left|\varphi_{00}(\mathbf{r})\right|^2 \left|S_p(b_p)\right|^2 \left(1 - \left|S_n(b_n)\right|^2\right), \tag{2.17}$$

$$\begin{aligned} \sigma_{EB} = \int d^2\mathbf{b}_d \Bigg(& \int d^3\mathbf{r} \left|\varphi_{00}\right|(\mathbf{r})^2 \left|S_p(b_p) S_n(b_n)\right|^2 \\ & - \left| \int d^3\mathbf{r} \left|\varphi_{00}(\mathbf{r})\right|^2 S_p(b_p) S_n(b_n) \right|^2 \Bigg), \end{aligned} \tag{2.18}$$

and the deuteron absorption cross section σ_{d-ABS} is defined as follows:

$$\sigma_{d-ABS} = \sigma_{REA} - \left(\sigma_{p-STR} + \sigma_{n-STR} + \sigma_{EB}\right). \tag{2.19}$$

2.5 Exciton model and Hauser-Feshbach model

In the present code system, the CCONE code [2.4] are used to calculate statistical decay components, i.e., pre-equilibrium and compound components.

In the original CCONE code, the calculation of the pre-equilibrium reaction is performed based on the formalism of the two-component exciton model by Kalbach [2.10 - 2.12] with some modifications. In addition, the CCONE code has recently been extended so as to treat multiple particle emission from pre-equilibrium process and to obtain spectrum in the laboratory system. The details of the two-component exciton models and its extensions are described in Refs. [2.4, 2.13]. In the

present code system, the latest version of CCONE are adopted and so the above extensions are available.

On the other hand, the Hauser-Feshbach models is used to calculate the compound nuclear reaction. In the CCONE code, the Hauser-Feshbach models including width fluctuation correction (WFC) is applied and multi-particle emission from the compound nucleus is included with conservation of the spin and parity. As it is for the exciton models, the details of the Hauser-Feshbach models used in the CCONE code are described in Ref. [2.4].

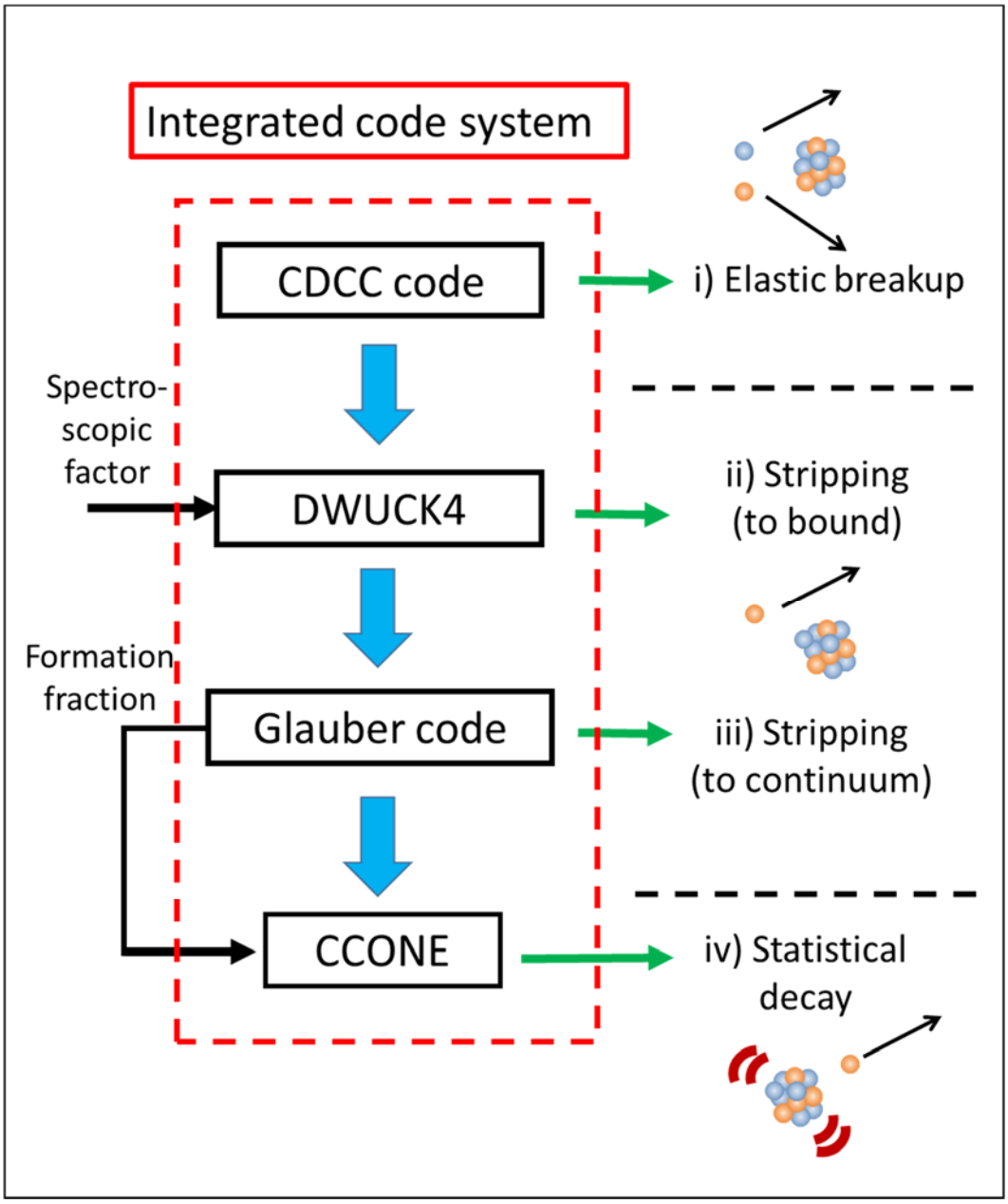

Fig. 2.1 Structure of the integrated code system

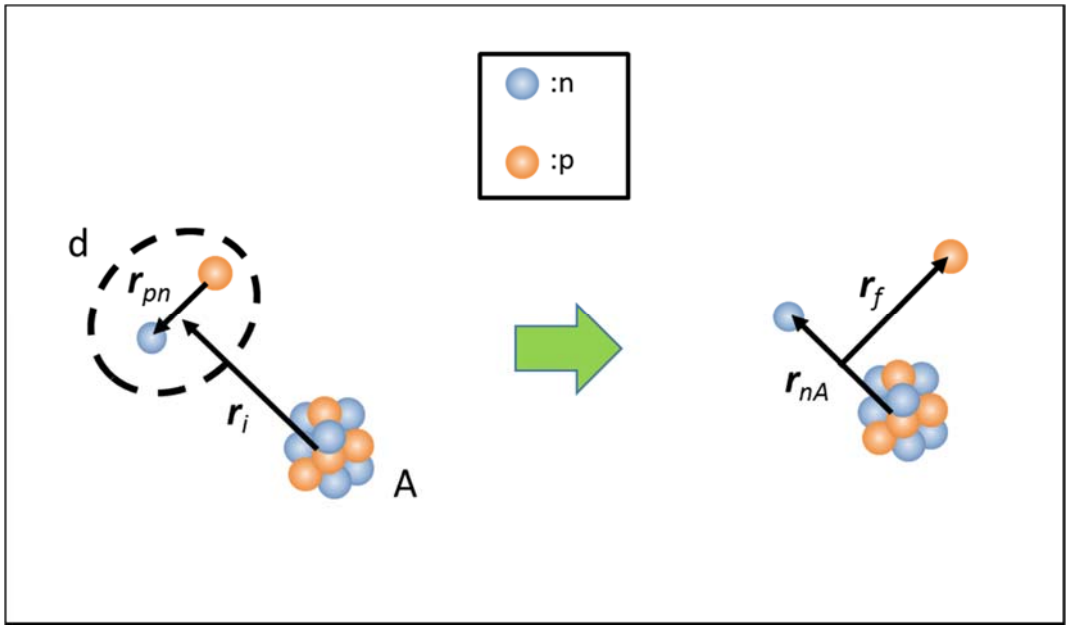

Fig. 2.2 Coordinate system in the DWBA calculation

Bibliography

[2.1] M. Yahiro, K. Ogata, T. Matsumoto, K. Minomo, "The continuum discretized coupled-channels method and its applications", Prog. Theor. Exp. Phys. **2012**, 01A206 (2012), and references therein.

[2.2] P. D. Kunz, computer code DWUCK4 (1974), http://spot.colorado.edu/~kunz/DWBA.html.

[2.3] T. Ye, S. Hashimoto, Y. Watanabe, K. Ogata, M. Yahiro, "Analysis of inclusive (*d*,*xp*) reactions on nuclei from ^{9}Be to ^{238}U at 100 MeV", Phys. Rev. C **84**, 054606 (2011).

[2.4] O. Iwamoto, "Development of a comprehensive code for nuclear data evaluation, CCONE, and validation using neutron-induced cross sections for uranium isotopes", J. Nucl. Sci. Technol. **44**, 687-697 (2007).

[2.5] K. Shibata, O. Iwamoto, T. Nakagawa, N. Iwamoto, A. Ichihara, S. Kunieda, S. Chiba, K. Furutaka, N. Otuka, T. Ohsawa, T. Murata, H. Matsunobu, A. Zukeran, S. Kamada, J. Katakura, "JENDL-4.0: A new library for nuclear science and engineering", J. Nucl. Sci. Technol. **48**, 1-30 (2011).

[2.6] Y. Iseri, M.Yahiro, M. Kamimura, "Coupled-Channels Approach to Deuteron and ^{3}He Breakup Reactions", Prog. Theor. Phys. Suppl. **89**, 84-117 (1986).

[2.7] G. G. Ohlsen, "Kinematic relations in reactions of the form A + B → C + D + E", Nucl. Instr. Meth. **37**, 240-248 (1965).

[2.8] C. A. Bertulani, P. G. Hansen, "Momentum distributions in stripping reactions of radioactive projectiles at intermediate energies", Phys. Rev. C **70**, 034609 (2004).

[2.9] K. Hencken, G. Bertsch, H. Esbensen, "Breakup reactions of the halo nuclei ^{11}Be and ^{8}B", Phys. Rev. C **54**, 3043-3050 (1996).

[2.10] C. Kalbach, "Two-component exciton model: Basic formalism away from shell closures", Phys. Rev. C **33**, 818-833 (1986).

[2.11] C. Kalbach, “Surface effects in the exciton model of preequilibrium nuclear reactions”, Phys. Rev. C **32**, 1157-1168 (1985).

[2.12] C. Kalbach, “Consistent exciton model calculations with shell structure, pairing and isospin effects”, J. Phys. G. **21**, 1519 (1995).

[2.13] O. Iwamoto, “Extension of a nuclear reaction calculation code CCONE toward higher incident energies – multiple preequilibrium emission, and spectrum in laboratory system”, J. Nucl. Sci. Tech. **50**, 409-418 (2013).

Chapter 3

Systematic investigation of spectroscopic factors for (*d*, *p*) reactions

As described in the Chapter 2, in the integrated code system, Distorted Wave Born Approximation (DWBA) is used to calculate stripping reactions to bound states in the residual nuclei. In this chapter, we perform systematic investigation of spectroscopic factor (SF) which is necessary to determine the absolute values of DWBA calculations.

3.1 Earlier works on systematic investigation of spectroscopic factors

First of all, there are several earlier works on systematic investigation of neutron SFs. Liu et al. [3.1] extracted the SF values of $^{12}C(d,p)^{13}C_{g.s.}$ and $^{13}C(p,d)^{12}C_{g.s.}$ reactions for incident energies up to 60 MeV and investigated the dependence of optical potentials (OPs) used in DWBA calculations on the SF value. Tsang et al. [3.2] analyzed a lot of experimental data and extracted the ground state neutron SFs for 80 nuclei from Li to Cr isotopes. Most of the extracted SF values were reproduced by Large-Basis Shell-Model (LB-SM) predictions within 20%. Both the analyses were conducted only for the ground-state to ground-state transitions. SF values for excited states in the residual nuclei are also necessary in nuclear data evaluation of deuteron induced reactions. In addition, it is not clear whether or not the SF values extracted by conventional DWBA analyses are independent of incident energy if the range of incident energy is extended over 60 MeV. Thus, it is interesting

to investigate systematically the SF values deduced by DWBA analyses for wide ranges of deuteron incident energy and target mass number. In the following, therefore, SFs for the (*d*,*p*) reactions on ^{12}C, ^{27}Al, ^{40}Ca, and ^{58}Ni for incident deuteron energies up to 100 MeV are extracted systematically by fitting theoretical DWBA calculations to the exiting experimental data.

3.2 Input parameters of DWBA calculation

The DWBA differential cross section for the (*d*,*p*) reaction leading to the bound state *i* is given by

$$\frac{d\sigma^{DWBA}_{bound,i}}{d\Omega}(E_d) = \frac{D_0^2}{10^4}\frac{2J_i+1}{2J_A+1}\frac{S_i}{2j+1}\frac{d\sigma^{DWUCK4}_{bound,i}}{d\Omega}(E_d), \qquad (3.1)$$

where E_d is the incident deuteron energy, D_0 is a constant used in zero-range approximation, J_A and J_i are the spins of target nucleus and *i*-th state of residual nucleus, respectively, S_i is the spectroscopic factor for each state, j is the spin of transferred neutron, and $d\sigma^{DWUCK\,4}_{bound\,,i}/d\Omega$ is the differential cross section calculated with the DWUCK4 code [3.3]. The spectroscopic factor S_i is extracted by fitting the calculated DWBA cross section to the corresponding experimental one in the small angular region where neutron stripping process is dominant.

Input parameters used in DWUCK4 calculations are listed in Table 3.1. The parameters except OPs are determined with reference to Refs. [3.1, 3.2]. Global OPs of Koning and Delaroche (KD) [3.4] are employed for proton and neutron. The adiabatic potential based on nucleon OPs of KD is used for deuteron [3.5]: hereafter this OP option will be referred to as "Adiabatic". The other OP option with global deuteron OP of An and Cai [3.6] is also used to assess the effect of the adiabatic potential, which will be called as "An-Cai" option. The Woods-Saxon shape with fixed radius and diffuseness parameters given in Table 3.1 is assumed for neutron binding potential. No spin-orbit coupling is considered as in Refs.

[3.1, 3.2], because we have confirmed that that DWUCK4 calculations vary only 5% or less even if spin-orbit coupling is included. Moreover, the relativistic correction is not considered because the effect is within a few percent at 100 MeV.

3.3 Analyses of differential cross sections for (*d*,*p*) reactions

Experimental differential (*d*,*p*) cross sections available in the wide range of incident energy are used to investigate the incident energy dependence of SFs. They are for the reactions ^{12}C(*d*,*p*)^{13}C$_{g.s.}$, ^{27}Al(*d*,*p*)^{28}Al$_{g.s.}$, ^{40}Ca(*d*,*p*)^{41}Ca$_{g.s.}$, and ^{58}Ni(*d*,*p*)^{59}Ni$_{g.s.}$. In the present analyses, the SF values are extracted by fitting the DWBA calculations to the experimental data using the least-square method in the angular range of $\theta_{c.m.} < 60^{o}$. In the same manner as Ref. [3.1], the statistical decay contribution from compound nuclei is not considered because this component is not so large at forward angles. Our preliminary calculation showed that the effect on extracted SF values is about 25% in the largest case of the ^{12}C(*d*,*p*)^{13}C$_{g.s.}$ at 7.15 MeV and it reaches to a few percent in the case of incident energies larger than 10 MeV or target nuclei heavier than ^{12}C as described in Ref. [3.7].

Figure 3.1 shows comparison of calculated and experimental differential cross sections for the ^{12}C(*d*,*p*)^{13}C$_{g.s.}$ reaction in the incident energy range from 7.15 MeV to 56 MeV. All of experimental data are taken from the works cited in Ref. [3.1]. The calculation results with two optical potential options, “Adiabatic” and “An-Cai”, are shown by solid and dashed lines, respectively. Both the calculations show good agreement with the experimental data at small angles to the same extent.

In Fig. 3.2, the results for the ^{27}Al(*d*,*p*)^{28}Al$_{g.s.}$ reaction are shown in the incident energy range from 6 MeV to 23 MeV. Experimental data are taken from Refs. [3.8 - 3.10]. The contribution of the transition to the first excited state of ^{28}Al (E_{ex} = 0.031 MeV) is included only at 23 MeV [3.10]. From the experimental data at 6 MeV [3.8] and 12 MeV [3.9], the

magnitude of this component is estimated to be about half of the transition to the ground state. The SF value at 23 MeV is extracted under the same estimation. It should be noted that two components of angular momentum transfer, l = 0 and 2, are considered in the ^{27}Al(d,p)^{28}Al$_{g.s.}$ reaction in the same way as in Refs. [3.8 - 3.10]. As is the case in Fig. 3.1, the calculations reproduce the experimental data at forward angles fairly well.

Figures 3.3 and 3.4 are the results for the ^{40}Ca(d,p)^{41}Ca$_{g.s.}$ and the ^{58}Ni(d,p)^{59}Ni$_{g.s.}$ reaction in the incident energy range up to 56 MeV, respectively. Experimental data are taken from Refs. [3.11 - 3.18] for ^{40}Ca(d,p)^{41}Ca$_{g.s.}$ and Refs. [3.19 - 3.22] for ^{58}Ni(d,p)^{59}Ni$_{g.s.}$. Through all the DWBA analyses, the calculations show good agreement with experimental data and relatively those with “Adiabatic” option look better. The extracted SF values are given and discussed in the later section 3.4.

3.4 Extraction of spectroscopic factors at high incident energies

For deuteron nuclear data evaluation, it is of great importance to investigate SF values over the wide range of incident energy. However, there is no experimental differential cross section for (d,p) reactions in the energy range higher than 56 MeV as shown in Figs. 3.1 to 3.4. On the other hand, experimental data of DDXs for the (d,xp) reactions on ^{12}C, ^{27}Al and ^{58}Ni in this energy range do exist [3.23 - 3.27]. In these DDXs, overlapped peaks are observed in the high emission energy region at forward angles. These peaks correspond to the contributions from the stripping reaction to bound states in residual nuclei. It should be noted that the SF values can be obtained using the experimental data of DDXs from the (d,xp) reactions if we assume that the incident energy dependence is same for all the final states. We have therefore attempted to extract SF values in the incident energy region between 56 MeV to 100 MeV using the experimental DDXs in the following manner.

First of all, the experimental DDXs are integrated over the energy of emitted protons around the observed peaks to obtain the differential cross sections with respect to angle as shown in Fig 3.5.

Next, the spectroscopic factor $S_i(E_0)$ is deduced for each discrete state i at the incident energy E_0 where experimental differential cross sections for as many final states as possible are available for ^{12}C [3.28], ^{27}Al [3.8], and ^{58}Ni [3.22]. The number of final states at E_0 is defined as I_0. The values of E_0 and I_0 for ^{12}C, ^{27}Al, and ^{58}Ni are listed in Table 3.2. Using the extracted $S_i(E_0)$, DWBA differential cross sections are calculated for all final states up to I_0 using Eq. (3.1) at other incident energy E_d where the experimental DDXs exist. The calculated DWBA differential cross sections are summed from i = 1 up to I_0. The summed result can be compared to the experimental data integrated over emission energy around the observed peaks.

Then, the normalization constant $N(E_d)$ is determined so that the DWBA calculation reproduces the experimental data at small angles reasonably well as shown in Fig. 3.6. Finally, the SF value for each final state at E_d is deduced as the product of $N(E_d)$ and $S_i(E_0)$ under the assumption that the incident energy dependence is same for all the final states. In this way, the SF values at incident energies between 56 MeV and 100 MeV are extracted from DWBA analyses using DDXs data.

3.5 Results and discussion about spectroscopic factors

First, the SF values for the ^{12}C(d,p)^{13}C$_{g.s.}$ reaction extracted from the present analysis are presented in Fig. 3.7 and Table 3.3. The SF values extracted by Liu et al. [3.1] are also shown for comparison. In Fig. 3.7, the SF values extracted from the analyses of differential cross sections and the DDXs are plotted as solid circles and solid squares, respectively. In addition, the horizontal dashed line denotes a theoretical SF value obtained from shell-model calculation (0.61) [3.2]. As seen in Fig. 3.7, the present SF values show similar energy dependence to the previous SF

values [3.1] in the energy range up to 50MeV. Furthermore, one notices that the absolute SF value depends strongly on deuteron OPs used in DWBA calculation. The difference between “Adiabatic” and “An-Cai” is similar to that between “Liu (CH)” and “Liu (DWBA)”, where “CH” and “DWBA” denote the use of adiabatic deuteron OP and global deuteron OP in Ref. [3.1], respectively. In both the cases, the absolute SF values for adiabatic OPs are smaller than those for global OPs. In addition, the SF values extracted from ^{13}C(p,d)^{12}C$_{g.s.}$ pickup reactions at 63MeV are 0.26 to 0.43 depending on OPs used in DWBA calculation [3.29], which are much smaller than the SF values below 50 MeV and this decline trend with increasing energy seen over 50 MeV is similar to the energy dependence seen in the present work.

In Fig. 3.8 and Table 3.4, the SF values for the ^{27}Al(d,p)^{28}Al$_{g.s.}$ reaction are presented. As described in Sec. 3.2, two components of l = 0 and 2 are considered and the sum of two SF values is plotted. The horizontal dashed line denotes a theoretical SF value (0.60) obtained by a shell-model calculation cited in Ref. [3.2]. As in the ^{12}C(d,p)^{13}C$_{g.s.}$ reactions, the trend of the energy dependence is similar regardless of deuteron OPs and the absolute SF values get small in the case of adiabatic OPs.

Next, the SF values for the ^{40}Ca(d,p)^{41}Ca$_{g.s.}$ reaction are shown in Fig. 3.9 and Table 3.5. Since there is no experimental DDX for the ^{40}Ca(d,xp) reaction, the upper limit of incident energy is 56 MeV. The extracted SF values are distributed near unity. The SF physically means the degree of vacancy of the corresponding single particle orbit. In the ^{40}Ca(d,p)^{41}Ca$_{g.s.}$ reaction, the theoretical neutron SF value must be unity since ^{40}Ca is doubly closed shell nuclei and the independent particle model works well. In fact, a theoretical SF value obtained by a shell-model calculation cited in Ref. [3.2] is 1.0. Therefore, the present DWBA analysis seems reasonable. The general trend of the energy dependence is similar to that for two cases of ^{12}C and ^{27}Al.

Finally, the SF values for the ^{58}Ni(d,p)^{59}Ni$_{g.s.}$ reaction are presented in Fig. 3.10 and Table 3.6. The horizontal dashed line denotes a theoretical SF value (0.48) taken from Ref. [3.30]. In addition, the SF value extracted from experimental differential cross sections for (d,p) reactions at 56 MeV [3.22] and that extracted from experimental DDXs for (d,xp) reactions at 56 MeV [3.26] almost coincide with each other. This result indicates the validity of the present analysis with DDXs.

The present DWBA analysis reveals that the extracted SF values of all the four reactions have similar incident energy dependence. The steep rise of the SF values with decreasing energy below 10 MeV may be attributed partly to the effect of compound formation and resonances as discussed in the Ref. [3.1]. On the other hand, the reason is not clear for the gradual decrease of SF values with increasing energy. Finite range effect might be responsible partly for this trend because zero range approximation is used in the DWUCK4 code. Further study will be necessary to explain the incident energy dependence of the extracted SF values.

3.6 Empirical expression of the energy dependence

From the view point of nuclear data evaluation, we propose a practical way to consider the energy dependence of the SF values in the calculation of stripping reactions below. Based on the SF values extracted with "Adiabatic" option for the ^{12}C(d,p)^{13}C$_{g.s.}$ reaction, the following empirical expression describing the energy dependence is derived:

$$S_{\text{C-12,1}}(E_d) = -2.18\times10^{-6}E_d^3 + 3.19\times10^{-4}E_d^2 - 1.56\times10^{-2}E_d + 8.20\times10^{-1} \quad (3.2)$$

As seen in Fig. 3.11, the empirical SF values reproduce the SF values extracted from the DWBA analysis for ^{12}C fairly well. Since the energy dependence of SFs for the other reactions resembles that for the ^{12}C(d,p)^{13}C$_{g.s.}$, we assume the same energy dependence as Eq. (3.2) and

obtain the following empirical expression of SF values for the other reactions:

$$S_{k,i}(E_d) = F_{k,i} S_{\text{C-12,1}}(E_d), \tag{3.3}$$

where $F_{k,i}$ is a scaling factor depending on target nucleus k and the excited states i of residual nucleus. As shown in Fig. 3.11, the empirical SF values are in reasonable agreement with the SF values extracted with "Adiabatic" option. The obtained $F_{k,1}$ factor are 0.6 for ^{27}Al(d,p)^{28}Al$_{\text{g.s.}}$, 1.4 for ^{40}Ca(d,p)^{41}Ca$_{\text{g.s.}}$, and 0.8 for ^{58}Ni(d,p)^{59}Ni$_{\text{g.s.}}$, respectively. Since the SF does not necessarily change smoothly along with target mass number A and atomic number Z, we were not able to express $F_{k,i}$ as a function of A and Z like conventional global OPs. However, one can apply Eqs. (3.2) and (3.3) to the cross section calculation for (d,p) stripping reactions for incident energies up to 100 MeV if one can obtain the SF value at a certain incident energy experimentally or theoretically. This will be useful for future deuteron nuclear data evaluation.

3.7 Summary

Neutron spectroscopic factors for the (d,p) reactions on ^{12}C, ^{27}Al, ^{40}Ca, and ^{58}Ni for incident deuteron energies up to 100 MeV were derived by DWBA analyses. It was shown that the absolute value of SF depends strongly on deuteron OPs used in DWBA calculation. In addition, the extracted SFs showed similar incident energy dependence among all the target nuclei. Finally, an empirical expression describing the energy dependence was deduced. The values of SFs obtained here are used for the DWBA calculations in the following chapters 4 and 5.

Table 3.1 Summary of input parameters used in DWUCK4.

Proton potential	Koning-Deraloche [3.4]
Deuteron potential	Adiabatic [3.5] from KD (“Adiabatic” option)
	An-Cai [3.6] (“An-Cai” option)
Neutron binding potential	Woods-Saxon form
	r_0 = 1.25 [fm], a = 0.65 [fm]
Finite range correction factor [fm]	0.7457
Zero-range constant D_0^2 [MeV^{2}fm^3]	1.5×10^4
Nonlocality parameters	p:0.85, d:0.54

Table 3.2 List of the values of E_0 and I_0.

Reaction	E_0 [MeV]	I_0
^{12}C(d,p)^{13}C	56	4
^{27}Al(d,p)^{28}Al	6	35
^{58}Ni(d,p)^{59}Ni	56	35

Table 3.3 List of spectroscopic factors for the $^{12}C(d,p)^{13}C_{g.s.}$ reaction extracted from the present analysis and the one by Liu et al. [3.1].

E_d [MeV]	Adiabatic	An-Cai	Liu(JLM)	Liu(CH)	Liu(DWBA)
7.15	0.75	0.92	0.89	0.93	0.94
8.9	0.71	0.89	0.80	0.90	0.91
10.2	0.68	0.83	0.68	0.79	0.81
11.8	0.71	0.77	0.61	0.74	0.77
12	0.63	0.76	0.50	0.63	0.68
12	0.71	0.79	0.75	0.85	0.86
12.4	0.70	0.81	0.63	0.74	0.78
14.7	0.62	0.75	0.61	0.74	0.79
14.8	0.61	0.72	0.64	0.75	0.78
15	0.68	0.79	0.53	0.67	0.74
16.6	0.56	0.70	0.48	0.59	0.66
19.6	0.62	0.77	0.52	0.65	0.76
25.9	0.66	0.78	0.59	0.69	0.79
30	0.58	0.72	0.52	0.65	0.79
51	0.57	0.79	0.66	0.82	1.06
56	0.55	0.76	-	-	-
100(DDX)	0.28	0.34	-	-	-

Table 3.4 List of spectroscopic factors for the ^{27}Al(d,p)^{28}Al$_{g.s.}$ reaction extracted from the present analysis.

	Adiabatic		
E_d [MeV]	$l = 0$	$l = 2$	Sum
6	0.52	0.13	0.65
12	0.43	0.10	0.53
23	0.36	0.08	0.44
25.5(DDX)	0.31	0.08	0.39
56(DDX)	0.28	0.07	0.35
80(DDX)	0.24	0.06	0.30
100(DDX)	0.11	0.03	0.14

	An-Cai		
E_d [MeV]	$l = 0$	$l = 2$	Sum
6	0.69	0.21	0.90
12	0.55	0.17	0.72
23	0.47	0.14	0.61
25.5(DDX)	0.41	0.13	0.54
56(DDX)	0.37	0.11	0.49
80(DDX)	0.28	0.08	0.36
100(DDX)	0.14	0.04	0.18

Table 3.5 Same as Table 3.4 but for the ^{40}Ca(d,p)^{41}Ca$_{g.s.}$ reaction.

E_d [MeV]	Adiabatic	An-Cai
5	1.14	1.20
7	1.04	1.11
8	0.96	1.01
9	1.06	1.08
10	1.01	1.01
11	0.89	0.88
11.8	0.89	0.87
12	0.97	0.95
12.8	0.97	0.94
14.3	0.96	0.93
20	0.99	0.97
56	0.85	0.93

Table 3.6 Same as Table 3.4 but for the ^{58}Ni(d,p)^{59}Ni$_{g.s.}$ reaction.

E_d [MeV]	Adiabatic	An-Cai
7	0.52	0.68
9	0.51	0.64
10	0.48	0.61
56	0.47	0.59
56(DDX)	0.46	0.57
80(DDX)	0.32	0.38
100(DDX)	0.26	0.30

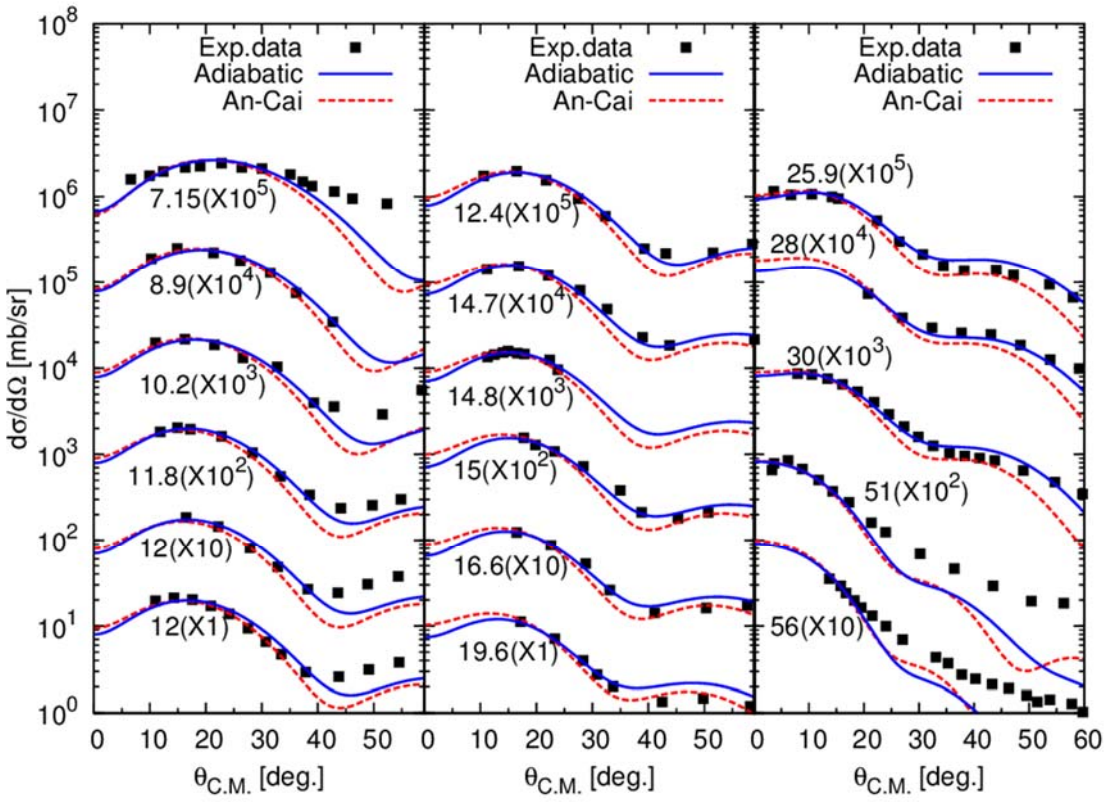

Fig. 3.1 Calculated and experimental differential cross sections for the $^{12}C(d,p)^{13}C_{g.s.}$ reaction for incident energies from 7.15 to 56 MeV.

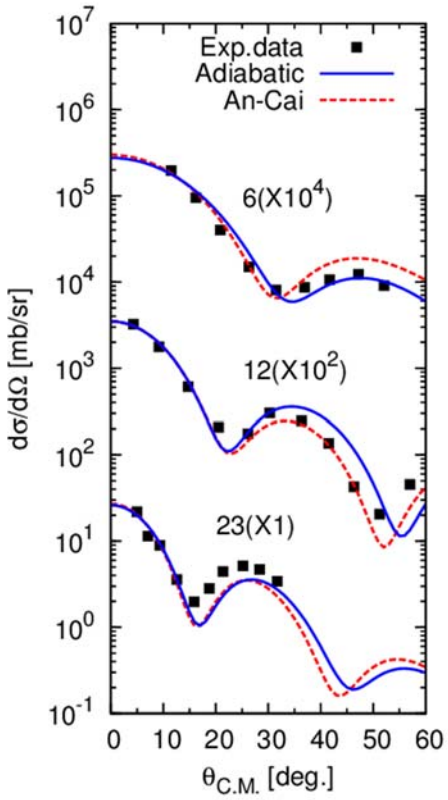

Fig. 3.2 Same as Fig. 3.1 but for the ^{27}Al(d,p)^{28}Al$_{g.s.}$ reaction for incident energies from 6 to 23 MeV. The contribution of the transition to the first excited state (E_{ex} = 0.031 MeV) is included only at 23 MeV.

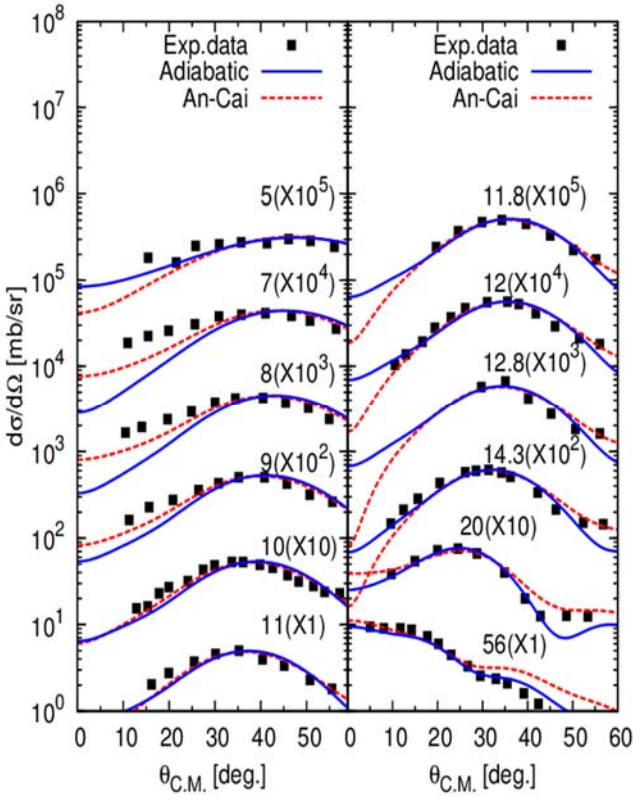

Fig. 3.3 Same as Fig. 3.1 but for the ^{40}Ca(d,p)^{41}Ca$_{g.s.}$ reaction for incident energies from 5 to 56 MeV.

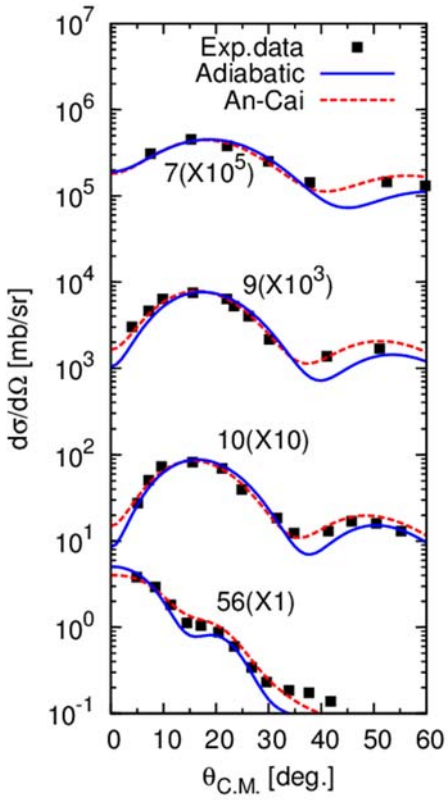

Fig. 3.4 Same as Fig. 3.1 but for the ^{58}Ni(d,p)^{58}Ni$_{g.s.}$ reaction for incident energies from 7 to 56 MeV.

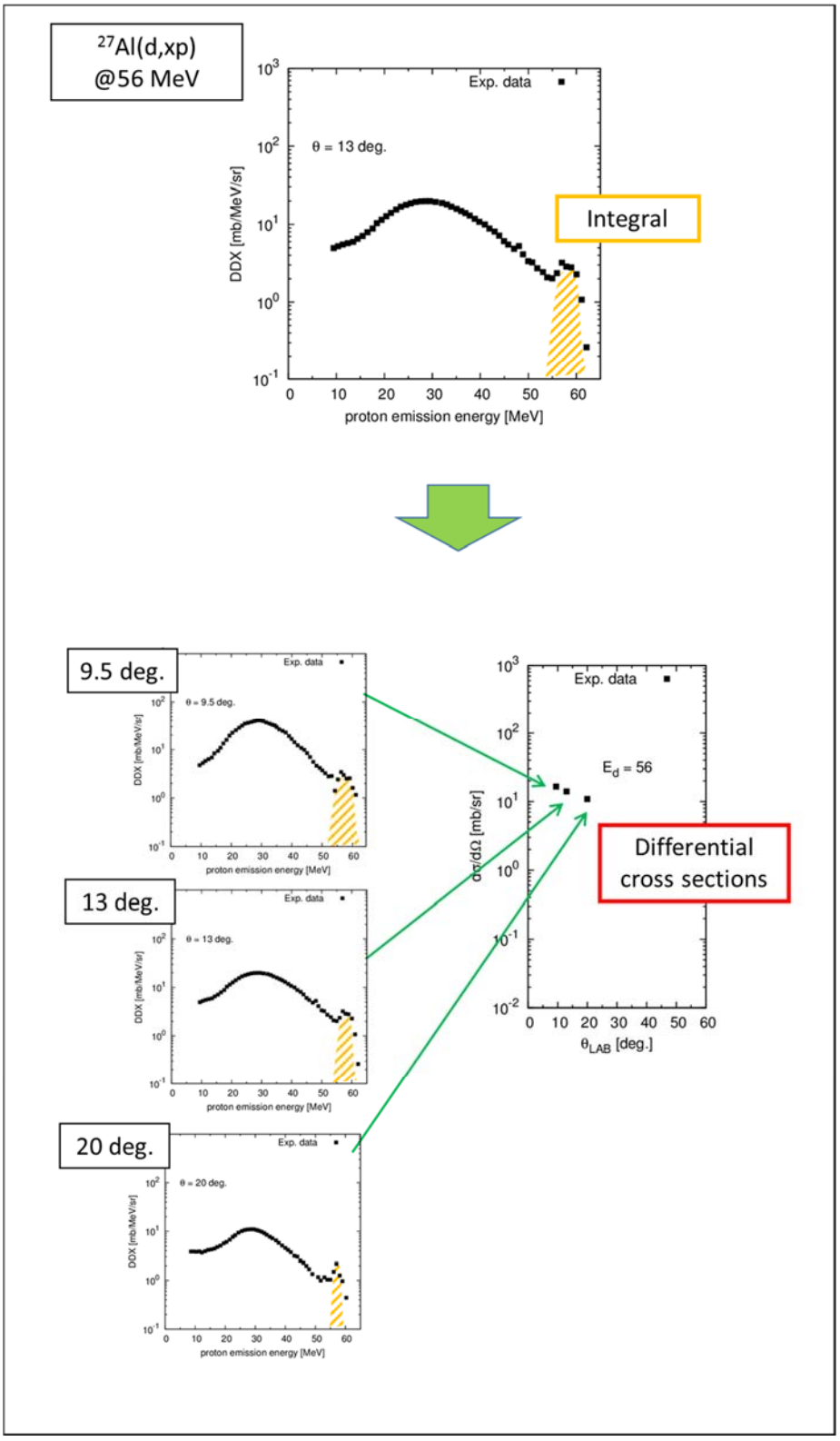

Fig 3.5 Differential cross sections obtained by integral of high energy peak observed in the experimental DDX data.

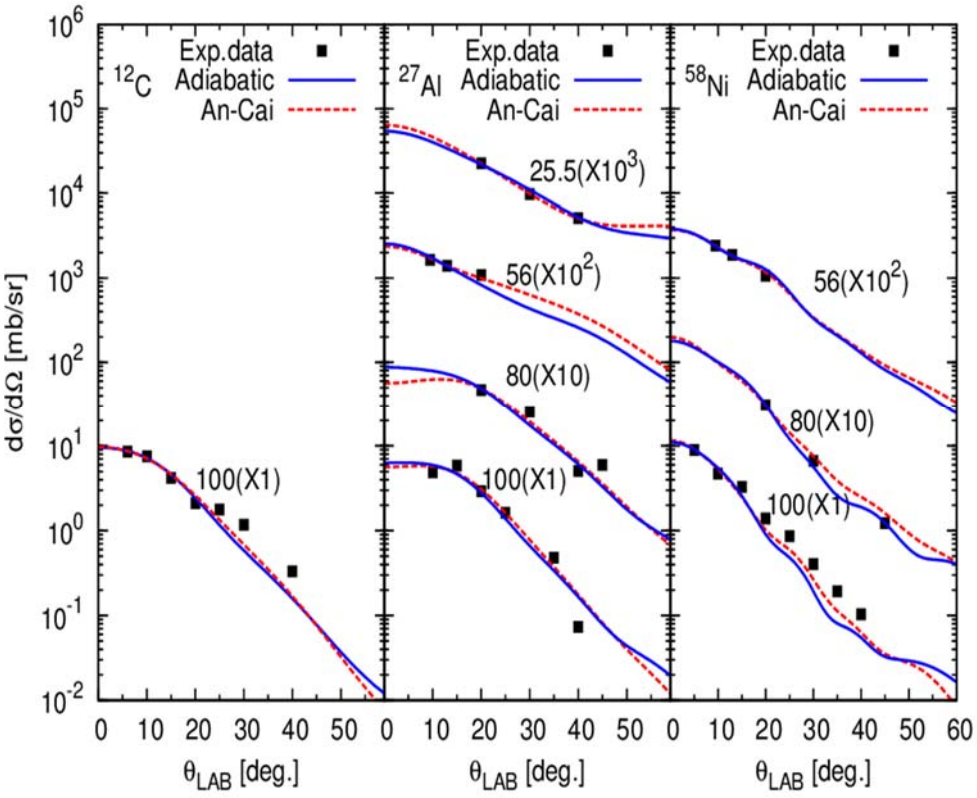

Fig. 3.6 Comparison of experimental and DWBA differential cross sections corresponding to overlapped peaks seen in the high emission energy region in (*d*,*xp*) spectra. The integral intervals are from the proton emission energy corresponding to the ground state to that corresponding to the I_0 given by Table 3.2.

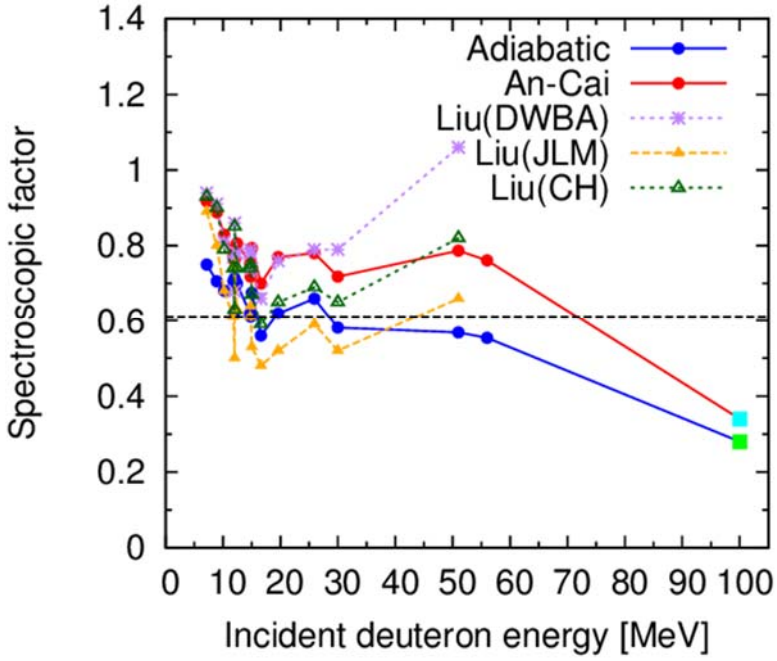

Fig. 3.7 Spectroscopic factors for the $^{12}C(d,p)^{13}C_{g.s.}$ reaction extracted from the present analysis and the past work [3.1]. Solid circles and solid squares denote the spectroscopic factors extracted from analyses of differential cross sections and DDXs, respectively. Horizontal dashed line represents a theoretical spectroscopic factor.

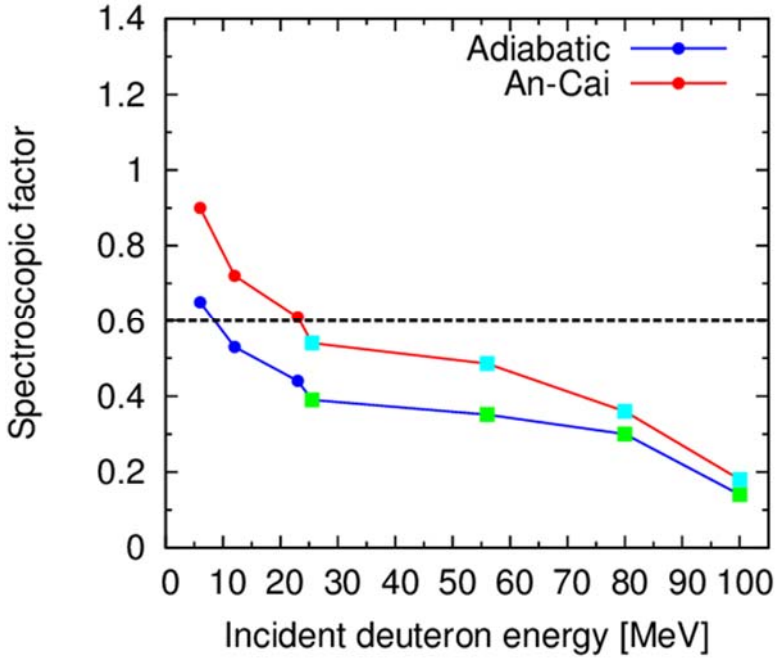

Fig. 3.8 Spectroscopic factors for the ^{27}Al(d,p)^{28}Al$_{g.s.}$ reaction extracted from the present analysis.
Solid circles and solid squares denote the spectroscopic factors extracted from analyses of differential cross sections and DDXs, respectively.
Horizontal dashed line represents a theoretical spectroscopic factor.

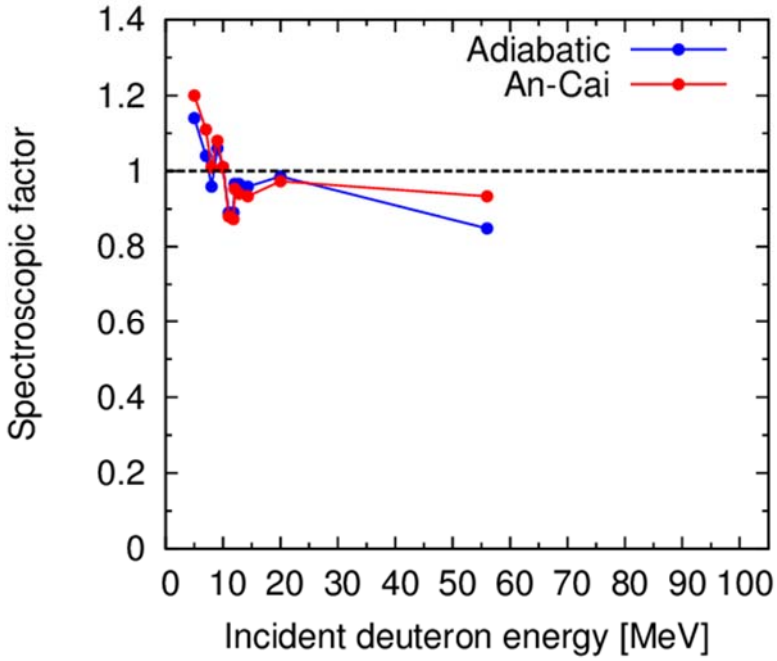

Fig. 3.9 Same as Fig. 3.8 but for the ^{40}Ca(d,p)^{41}Ca$_{g.s.}$ reaction.

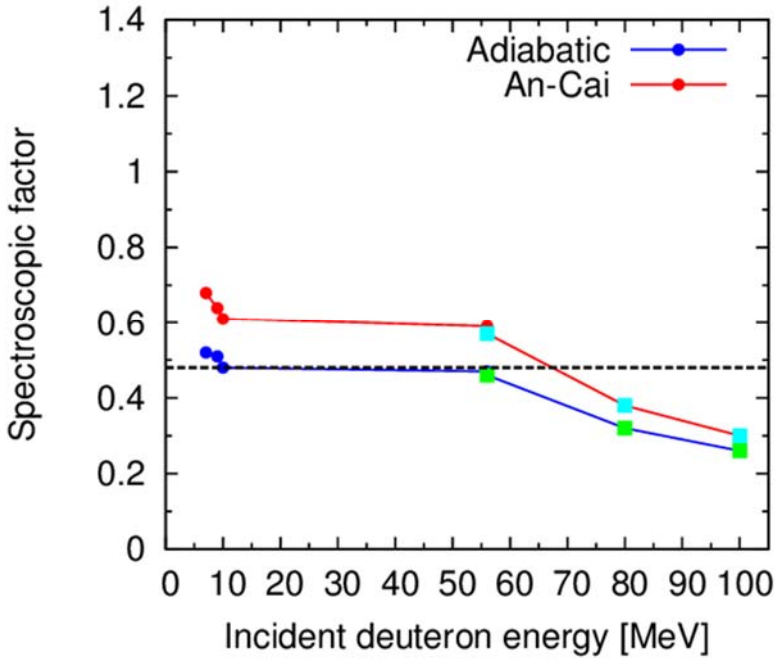

Fig. 3.10 Same as Fig. 3.8 but for the ^{58}Ni(d,p)^{59}Ni$_{g.s.}$ reaction.

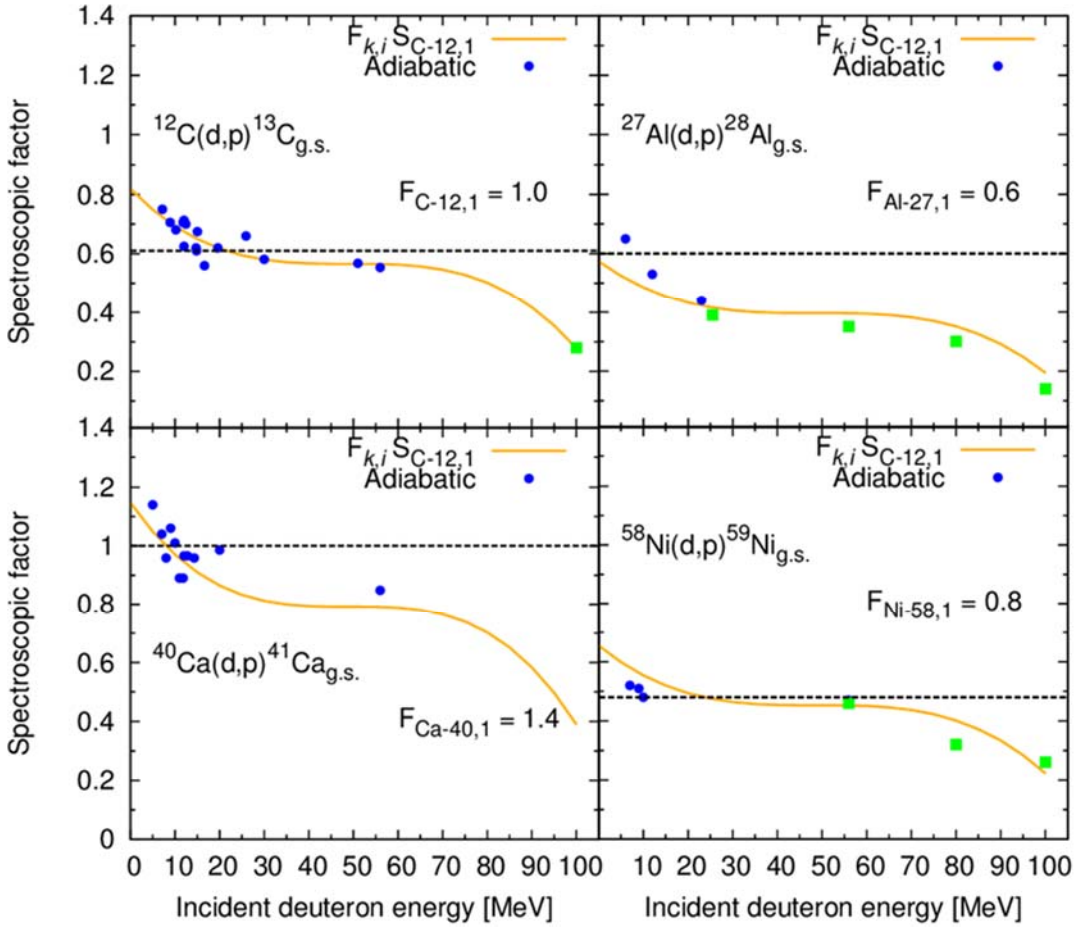

Fig. 3. 11 Comparison between spectroscopic factors extracted from DWBA analysis and empirical spectroscopic factors.
Solid circles and solid squares denote the spectroscopic factors extracted from analyses of differential cross sections and DDXs, respectively.
Horizontal dashed lines represent theoretical spectroscopic factors.

Bibliography

[3.1] X. D. Liu, M. A. Famiano, W. G. Lynch WG, M. B. Tsang, J. A. Tostevin, "Systematic extraction of spectroscopic factors from $^{12}C(d,p)^{13}C$ and $^{13}C(p,d)^{12}C$ reactions", Phys. Rev. C **69**, 064313 (2004).

[3.2] M. B. Tsang, J. Lee, W. G. Lynch, "Survey of ground state neutron spectroscopic factors from Li to Cr isotopes", Phys. Rev. Lett. **95**, 222501 (2005).

[3.3] P. D. Kunz, computer code DWUCK4 (1974), http://spot.colorado.edu/~kunz/DWBA.html.

[3.4] A. J. Koning, J. P. Delaroche, "Local and global nucleon optical models from 1 keV to 200 MeV", Nucl. Phys. A **713**, 231-310 (2003).

[3.5] D. G. Madland, "Recent results in the development of a global medium-energy nucleon-nucleus optical-model potential", Proc. Specialists' Meeting on Preequilibrium Nuclear Reactions, 103-110, Semmering, Austria, 10-12 Feb (1988).

[3.6] H. An, C. Cai, "Global deuteron optical model potential for the energy range up to 183 MeV", Phys. Rev. C **73**, 054605 (2006).

[3.7] M. Avrigeanu, W. Oertzen, R. A. Forrest, A. C. Obreja, F. L. Roman, V. Avrigeanu, "Analysis of deuteron elastic scattering and induced activation cross-sections of light and medium nuclei for IFMIF EVEDA", Fusion Eng. Des. **84**, 418-422 (2009).

[3.8] S. Chen, J. Rapaport, H. Enge, W. W. Buechner, "Level structure of ^{28}Al", Nucl. Phys. A **197**, 97-105 (1972).

[3.9] T. P. G. Carola, J. G. Van Der Baan, "Investigation of the $^{27}Al(d,p)^{28}Al$ reaction at E_d = 12 MeV. Nucl. Phys. A **173**, 414-426 (1971).

[3.10] J. V. Maher, H. T. Fortune, G. C. Morrison, B. Zeidman, "Reaction ^{27}Al(d,p)^{28}Al reaction at E_d = 23 MeV", Phys. Rev. C **5**, 1313-1322 (1972).

[3.11] D. C. Kosher, W. Haeberli, "Vector analyzing power and cross section for ^{40}Ca(d,p)^{41}Ca from 5 to 11 MeV", Nucl. Phys. A **172**, 652-662 (1972).

[3.12] L. L. Lee, J. P. Schiffer, B. Zeidman, G. R. Satchler, R. M. Drisko, R. H. Bassel, "Ca^{40}(d,p)Ca^{41}, a test of the validity of the distorted-wave Born approximation", Phys. Rev. **136**, B971-B993 (1964).

[3.13] U. Schmidt-Rohr, R. Stock, P. Turek. "Die winkelverteilungen der protonen aus den reaktionen Be^{9}(d, p)Be^{10}, C^{12}(d, p)C^{13}, O^{16}(d, p)O^{17}und Ca^{40}(d, p)Ca^{41} bei 11.8 MeV", Nucl. Phys. **53**, 77-86 (1964).

[3.14] J. Dobes, "An absorption model for direct transfer reactions", Nucl. Phys. A **157**, 661-672 (1970).

[3.15] H. Niewodniczanski, J. Nurzynski, A. Strzalkowski, G. R. Satchler, "^{40}Ca(d,d), (d,d'), and (d,p) reactions with 12.8-MeV deuterons". Phys. Rev. **146**, 799-803 (1966).

[3.16] S. A. Hjorth, J. X. Saladin, G. R. Satchler, "Study of the Ca^{40}(d,p)Ca^{41} ground state reaction at E_d =14.3 MeV", Phys. Rev. **138**, B1425-B1433 (1965).

[3.17] F. J. Eckle, H. Lenske, G. Eckle, G. Graw, R. Hertenberger, H. Kader, H. J. Maie, F. Merz, H. Nann, P. Schiemenz, H. H. Wolter, "Investigation of single-particle strength distributions in a high-resolution ^{40}Ca(d,p) study at E_d = 20 MeV", Nucl. Phys. A **506**, 159-195 (1990).

[3.18] Y. Uozumi, N. Kikuzawa, T. Sakae, M. Matoba, K. Kinoshita, T. Sajima, H. Ijiri, N. Koori, M. Nakano, T. Maki, "Shell-model study of ^{40}Ca with the 56-MeV (d,p) reaction", Phys. Rev. C **50**, 263-274 (1994).

[3.19] E. R. Cosman, C. H. Paris, A. Sperduto, H. A. Enge, "Nuclear-reaction studies in the nickel isotopes: The $Ni^{58}(p,p')$ Ni^{59} and $Ni^{58}(d,p)Ni^{59}$ reactions", Phys. Rev. **142**, 673-686 (1966).

[3.20] H. D. Scott, "The application of distorted wave Born approximation calculations to the analysis of some (d, p) angular distributions", Nucl. Phys. **27**, 490-506 (1961).

[3.21] J. A. Aymer. H. R. Hiddleston, S. E. Darden, A. A. Rollefson, "Spin assignment in ^{59}Ni from the ^{58}Ni(d,p)^{59}Ni reaction", Nucl. Phys. A **207**, 596-608 (1973).

[3.22] O. Iwamoto, A. Nohtomi, Y. Uozumi, T. Sakae, M. Matoba, M. Nakano, T. Maki, N. Koori, "Single-particle states in ^{59}Ni with ^{58}Ni(d,p)^{59}Ni reaction at 56 MeV and neutron-bound-state complex potentials", Nucl. Phys. A **576**, 387-408 (1994).

[3.23] D. Lidikas, W. Mittig, H. Savajols, P. Roussel-Chomaz, S. V. Fortsch, J. J. Lawrie, G. F. Steyn, "Inclusive proton production cross sections in (*d*,*xp*) reactions induced by 100 MeV deuterons", Phys. Rev. C **63**, 014610 (2000).

[3.24] J. R. Wu, C. C. Chang, H. D. Holmgren, "Charged-particle spectra: 80 MeV deuterons on ^{27}Al and ^{58}Ni and 70 MeV deuterons on ^{90}Zr, ^{208}Pb, and ^{232}Th", Phys. Rev. C **19**, 370-390 (1979).

[3.25] U. Bechstedt, H. Machner, G. Baur, R. Shyam, C. Alderliesten, O. Bousshid, A. Djaloeis, P. Jahn, C. Mayer-Boricke, F. Rosel, D. Trautmann, "Experimental and theoretical study of continuous proton spectra from high-energy deuteron induced reactions", Nucl. Phys. A **343**, 221-233 (1980).

[3.26] N. Matsuoka, M. Kondo, A. Shimizu, N. Saito, S. Nagamachi, H. Sakaguchi, A. Goto, F. Ohtani, "Deuteron break-up in the field of nuclei at 56 MeV", Nucl. Phys. A **345**, 1-12 (1980).

[3.27] J. Pumpus, J. Bisplinghoff, J. Ernst, T. Mayer-Kuckuk, J. Rao Rama, G. Baur, F. Rosel, D. Trautmann, "Inclusive proton spectra from deuteron break-up: Theory and experiment", Nucl. Phys. A

311, 141-160 (1978).

[3.28] H. Hatanaka, N. Matsuoka, T. Saito, K. Hosono, M. Kondo, S. Kato, T. Higo, S. Matsuki, Y. Kaodota, K. Ogino, "Systematic study of the (d, p) reaction with 56 MeV polarized deuterons", Nucl. Phys. A **419**, 530-546 (1984).

[3.29] K. Hosono, M. Kondo, T. Saito, N. Matsuoka, S. Nagamachi, T. Noro, H. Shimizu, S. Kato, K. Okada, K. Ogino, Y. Kadota, "A study of the (p, d) reactions on A = 12-94 nuclei by 65 MeV polarized protons", Nucl. Phys. A **343**, 234-248 (1980).

[3.30] N. Auerbach, "Nuclear structure of the nickel isotopes", Phys. Rev. **163**, 1203-1218 (1967).

Chapter 4

Double differential cross sections for (*d*,*xp*) reactions

In this chapter, the code system we developed is applied to analysis of double-differential cross sections (DDXs) for (*d*,*xp*) reactions. For engineering design of deuteron accelerator neutron sources, DDXs for (*d*,*xn*) reactions are critically important. However, experimental data of DDXs for (*d*,*xn*) reactions are lack over wide ranges of target mass number and incident energy. On the other hand, experimental data of DDXs for (*d*,*xp*) reactions exist to some extent. To validate the employed physical models, therefore, we compare the calculation results with experimental data of DDXs for (*d*,*xp*) reactions instead of (*d*,*xn*) reactions.

4.1 Calculation method

In the present code system, DDXs of (*d*,*xp*) reactions are expressed by incoherent summation of three components:

$$\frac{d^2\sigma_{(d,xp)}}{dEd\Omega} = \frac{d^2\sigma_{BU}}{dEd\Omega} + \frac{d^2\sigma_{STR}}{dEd\Omega} + \frac{d^2\sigma_{SD}}{dEd\Omega} \tag{4.1}$$

where $d^2\sigma_{BU}/dEd\Omega$, $d^2\sigma_{STR}/dEd\Omega$, and $d^2\sigma_{SD}/dEd\Omega$ correspond to DDXs for elastic breakup reaction, neutron stripping reaction, and statistical decay, respectively. In these three components, elastic breakup components are directly calculated with the CDCC method as described in Ref. [4.1].

Neutron stripping reaction components are divided into the following two components:

$$\frac{d^2\sigma_{STR}}{dEd\Omega} = \frac{d^2\sigma_{continuum}}{dEd\Omega} + \frac{d^2\sigma_{bound}}{dEd\Omega}, \tag{4.2}$$

where $d^2\sigma_{continuum}/dEd\Omega$ and $d^2\sigma_{bound}/dEd\Omega$ correspond to DDXs for stripping reactions to continuum and to bound states, respectively. The latter DDXs are obtained by folding the calculated DWBA cross sections corresponding to each bound state with Gaussian function as follows:

$$\frac{d^2\sigma_{bound}}{dEd\Omega} = \sum_{i}^{I_0} \frac{1}{\sqrt{2\pi\sigma^2}} \exp\left(-\frac{(E-\mu_i)^2}{2\sigma^2}\right) \frac{d\sigma_{bound,i}^{DWBA}}{d\Omega} \tag{4.3}$$

where E is the proton emission energy, σ is the standard deviation representing experimental energy resolution, and μ_i is the emission energy corresponding to the i-th discrete peak. $d\sigma_{bound,i}^{DWBA}/d\Omega$ is the differential cross section calculated from Eq. (3.1).

The Glauber model cannot deal with individual transitions to bound states by stripping process and calculates the sum of stripping to both continuum and bound states as a continuous spectrum. Thus, DDXs calculated by the Glauber model and the DWBA approach overlap with each other in the high emission energy region including bound states. To avoid the double counting, the DDXs calculated by the Glauber model are cutoff near a bit lower emission energy than the broad peak by DWBA calculation. The remaining Glauber model component corresponding to $d^2\sigma_{continuum}/dEd\Omega$ in Eq. (4.2) is renormalized so that the total stripping component calculated by the Glauber model is conserved.

Statistical decay processes from compound nuclei are relatively complicated. We cannot calculate directly them with the CCONE code [4.2]. This difficulty is caused by the fact that three different compound nuclei are formed by absorption of either a neutron or a proton or both in the deuteron in the case of deuteron-induced reactions. A schematic picture of these processes is shown in Fig. 4.1. To solve this problem, we

calculate DDXs for statistical decay from those compound nuclei in the following way:

$$\frac{d^2\sigma_{SD}}{dEd\Omega} = R_d \frac{d^2\sigma^{CCONE}_{(d,xp)}}{dEd\Omega} + R_p \frac{d^2\sigma^{CCONE}_{(p,xp)}}{dEd\Omega} + R_n \frac{d^2\sigma^{CCONE}_{(n,xp)}}{dEd\Omega} \tag{4.4}$$

where R_d, R_p, and R_n denote the formation fractions of three different compound nuclei, and $d^2\sigma^{CCONE}_{(d,xp)}/dEd\Omega$, $d^2\sigma^{CCONE}_{(p,xp)}/dEd\Omega$, and $d^2\sigma^{CCONE}_{(n,xp)}/dEd\Omega$ are DDXs for (d,xp) , (p,xp) , and (n,xp) reactions calculated with CCONE code, respectively.

Each formation fraction in Eq. (4.4) are defined as follows:

$$R_d = \frac{\sigma_{d-ABS}}{\sigma_{REA}}, \quad R_p = \frac{\sigma_{p-STR}}{\sigma_{REA}}, \quad R_n = \frac{\sigma_{n-STR}}{\sigma_{REA}} \tag{4.5}$$

where σ_{d-ABS}, σ_{p-STR}, and σ_{n-STR} denote the cross sections of deuteron absorption, proton stripping, and neutron stripping, which are calculated with the Glauber model and σ_{REA} is the total reaction cross section calculated with the optical model implemented in CCONE code.

In the calculation of DDXs for (p,xp) and (n,xp) reactions with CCONE code, the incident energies of neutron and proton are fixed to half the deuteron incident energy. Strictly speaking, this approximation is not correct because either neutron or proton absorbed on stripping reaction has an energy distribution. However our preliminary calculation showed that there is not so much difference between the calculation results of the approximate case and those of the case where energy distribution is considered exactly [4.3]. We use this approximation for reduction of computation time for future cross section evaluation.

4.2 Input parameters of each calculation

In the calculation with the CDCC method and the Glauber model, the nucleon optical potentials (OPs) of target nucleus are necessary as input data. In the present work, we use Koning and Delaroche (KD) OPs [4.4] at half the incident deuteron energy both for proton and neutron.

The input parameters in DWBA calculations are the same as those of "Adiabatic" options given in Table 3.1. Necessary spectroscopic factor (SF) value, $S_{k,i}(E_d)$, at a certain incident energy E_d are given by Eqs. (3.2) and (3.3) in which $F_{k,i}$ is determined at E_0 so that $S_{k,i}(E_0)$ is equal to the SF value extracted from DWBA analysis. The extracted SF values for each i-th state at E_0 are listed in Table 4.1 for ^{12}C, Table 4.2 for ^{27}Al, and Table 4.3 for ^{58}Ni, respectively. In addition, Fig. 4.2 to 4.4 show the results of DWBA analysis at E_0 for ^{12}C [4.5], ^{27}Al[4.6], and ^{58}Ni[4.7], respectively.

The OPs used in the CCONE code are the global nucleon OPs of KD for proton and neutron and the adiabatic OP [4.8] for deuteron in a consistent way as in DWBA calculations. Default values in the CCONE code are used for other physical parameters such as level density parameters.

4.3 Calculation results and discussion

Figures 4.5 to 4.10 show comparisons between the calculated and experimental DDXs for (d,xp) reactions on ^{12}C, ^{27}Al, and ^{58}Ni at 56 [4.9] and 100 MeV [4.10], respectively. The present calculations reproduce fairly well both the shape and magnitude of the experimental (d,xp) spectra over wide ranges of target mass number and incident energy at small angles.

The characteristic broad peak is formed at approximately half the incident energy by proton emission via elastic breakup and neutron stripping processes. These components are calculated with the Kalbach empirical formula [4.11] in TALYS code [4.12], while they are calculated using physics-based models in the present code system. This indicates that it is essential to choose theoretical models to describe adequately both the breakup and stripping processes characteristic of deuteron-induced reactions. In addition, the peaks observed in the high emission energy region corresponding to stripping reactions to bound states are also reproduced well by DWBA approach. Although some sharp peaks are seen in the continuum region, they might be due to hydrogen contamination as described in Ref. [4.10].

Next, we investigate the applicability of the code system at lower incident energies. The result of the ^{27}Al (*d*,*xp*) reaction at 25.5 MeV [4.13] is presented in Fig. 4.11. Since relative contribution of the stripping reaction to bound states at low incident energies is larger than that at high incident energies, the peak structure observed in high emission energy region becomes more prominent than those in Figs. 4.5 to 4.10. Although the calculation overestimates the experimental data slightly in the continuum region at 30^{o}, they reproduce well the experimental peak structure.

4.4 Summary

The code system we developed was applied to analysis of double-differential cross sections (DDXs) for (*d*,*xp*) reactions instead of (*d*,*xn*) reactions. As the result of analysis, the calculation using the code system reproduced the measured DDXs for (*d*,*xp*) reactions on ^{12}C, ^{27}Al, and ^{58}Ni at 25.5, 56, and 100MeV fairly well. The results demonstrate that the reaction models used in the present calculations are valid for DDXs for (*d*,*xp*) reactions and will be applicable to evaluation of DDXs for (*d*,*xn*) reactions necessary for engineering design of accelerator neutron sources.

Table 4.1 List of spectroscopic factors for $^{12}C(d,p)^{13}C$ reactions extracted from the present analysis at E_0 = 56 MeV.

i	E_{ex} [MeV]	J_i^{π}	l	$S_{\text{C-12},i}$
1	0(g.s.)	$\frac{1}{2}^-$	1	0.55
2	3.089	$\frac{1}{2}^+$	0	0.43
3	3.684	$\frac{3}{2}^-$	1	0.11
4	3.854	$\frac{5}{2}^+$	2	0.39

Table 4.2 Same as Table 4.1 but for ^{27}Al(d,p)^{28}Al reactions at E_0 = 6 MeV.

i	E_{ex} [MeV]	J_i^{π}	l	$S_{\text{Al-27},i}$
1	0(g.s.)	3^+	0, 2	0.52, 0.13
2	0.031	2^+	0, 2	0.25, 0.06
3	0.972	0^+	2	0.10
4	1.014	3^+	0, 2	0.04, 0.24
5	1.373	1^+	2	0.12
6	1.620	1^+	0, 2	0.02, 0.19
7	2.139	2^+	0, 2	0.18, 0.19
8	2.201	1^+	2	0.22
9	2.272	4^+	2	0.18
10	2.486	2^+	0, 2	0.04, 0.06
11	2.582	5^+	0, 2	0.01, 0.05
12	2.656	4^+	2	0.22
13	3.012	0^+	2	0.09
14	3.105	1^+	2	0.08
15	3.296	3^+	0, 2	0.02, 0.06
16	3.347	2^+	0, 2	0.03, 0.03
17	3.465	4^-	1, 3	0.16, 0.25
18	3.591	3^-	1, 3	0.19, 0.28
19	3.671	3^+	0, 2	0.01, 0.05

Table 4.2 (*Continued.*)

i	E_{ex}[MeV]	J_i^{π}	l	$S_{\text{Al-27},i}$
20	3.709	$(2, 3)^+$	0, 2	0.22*, 0.15*
21	3.876	2^-	1, 3	0.09, 0.12
22	3.936	2^+	0, 2	0.02, 0.06
23	4.033	5^-	1, 3	0.01, 0.27
24	4.115	1^+	2	0.07
25	4.244	2^+	0, 2	0.05, 0.03
26	4.313	$(1, 3, 5)^+$	2	0.15*
27	4.462	$(2, 4)^+$	2	0.10*
28	4.691	3^-	1, 3	0.18, 0.04
29	4.739	$(0 - 5)^+$	2	0.25*
30	4.765	2^-	1, 3	0.19, 0.09
31	4.849	1^+	0, 2	0.01, 0.09
32	4.904	2^-	1, 3	0.14, 0.08
33	4.999	2^+	0, 2	0.01, 0.13
34	5.015	3^+	0, 2	0.01, 0.03
35	5.135	3^-	1, 3	0.12, 0.07

* The value of $(2J_i + 1)S_i$ is presented since J_i is not assigned.

Table 4.3 Same as Table 4.1 but for ^{58}Ni(d,p)^{59}Ni reactions at E_0 = 56 MeV.

i	E_{ex}[MeV]	J_i^{π}	l	$S_{\text{Ni-58},i}$
1	0(g.s.)	$\frac{3}{2}^-$	1	0.47
2	0.341	$\frac{5}{2}^-$	3	0.84
3	0.466	$\frac{1}{2}^-$	1	0.65
4	0.880	$\frac{3}{2}^-$	1	0.06
5	1.193	$\frac{5}{2}^-$	3	0.03
6	1.307	$\frac{1}{2}^-$	1	0.37
7	1.685	$\frac{5}{2}^-$	3	0.16
8	1.953	$\frac{7}{2}^-$	3	0.02
9	2.418	$\frac{3}{2}^-$	1	0.01
10	2.633	$\frac{7}{2}^-$	3	0.02
11	2.683	$\frac{5}{2}^-$	3	0.05
12	3.060	$\frac{9}{2}^+$	4	0.13
13	3.461	$\frac{3}{2}^-$	1	0.05
14	3.544	$\frac{5}{2}^+$	2	0.07
15	3.648	$\frac{5}{2}^-$	3	0.05

Table 4.3 (*Continued.*)

i	E_{ex}[MeV]	J_i^{π}	l	$S_{\text{Ni-58},i}$
16	3.866	$\frac{3^-}{2}$	1	0.05
17	4.036	$\frac{3^-}{2}$	1	0.04
18	4.154	-	1	0.24*
19	4.293	-	1	0.56*
20	4.328	-	4	0.05*
21	4.506	$\frac{5^+}{2}$	2	0.11
22	4.709	$\frac{9^+}{2}$	4	0.01
23	4.799	$\frac{5^+}{2}$	2	0.14
24	4.960	-	1	0.24*
25	5.149	$\frac{1^+}{2}$	0	0.08
26	5.213	$\frac{1^+}{2}$	2	0.06
27	5.429	$\frac{9^+}{2}$	4	0.07
28	5.458	$\frac{5^+}{2}$	2	0.01
29	5.569	$\frac{1^+}{2}$	0	0.04

* The value of $(2J_i + 1)S_i$ is presented since J_i is not assigned.

Table 4.3 (*Continued.*)

i	E_{ex} [MeV]	J_i^{π}	l	$S_{\text{Ni-58},i}$
30	5.692	$\frac{1^+}{2}$	0	0.19
31	5.894	$\frac{5^+}{2}$	2	0.04
32	6.206	$\frac{5^+}{2}$	2	0.07
33	6.305	$\frac{5^+}{2}$	2	0.09
34	6.375	-	0	0.28*
35	7.353	-	2	0.84*

* The value of $(2J_i + 1)S_i$ is presented since J_i is not assigned.

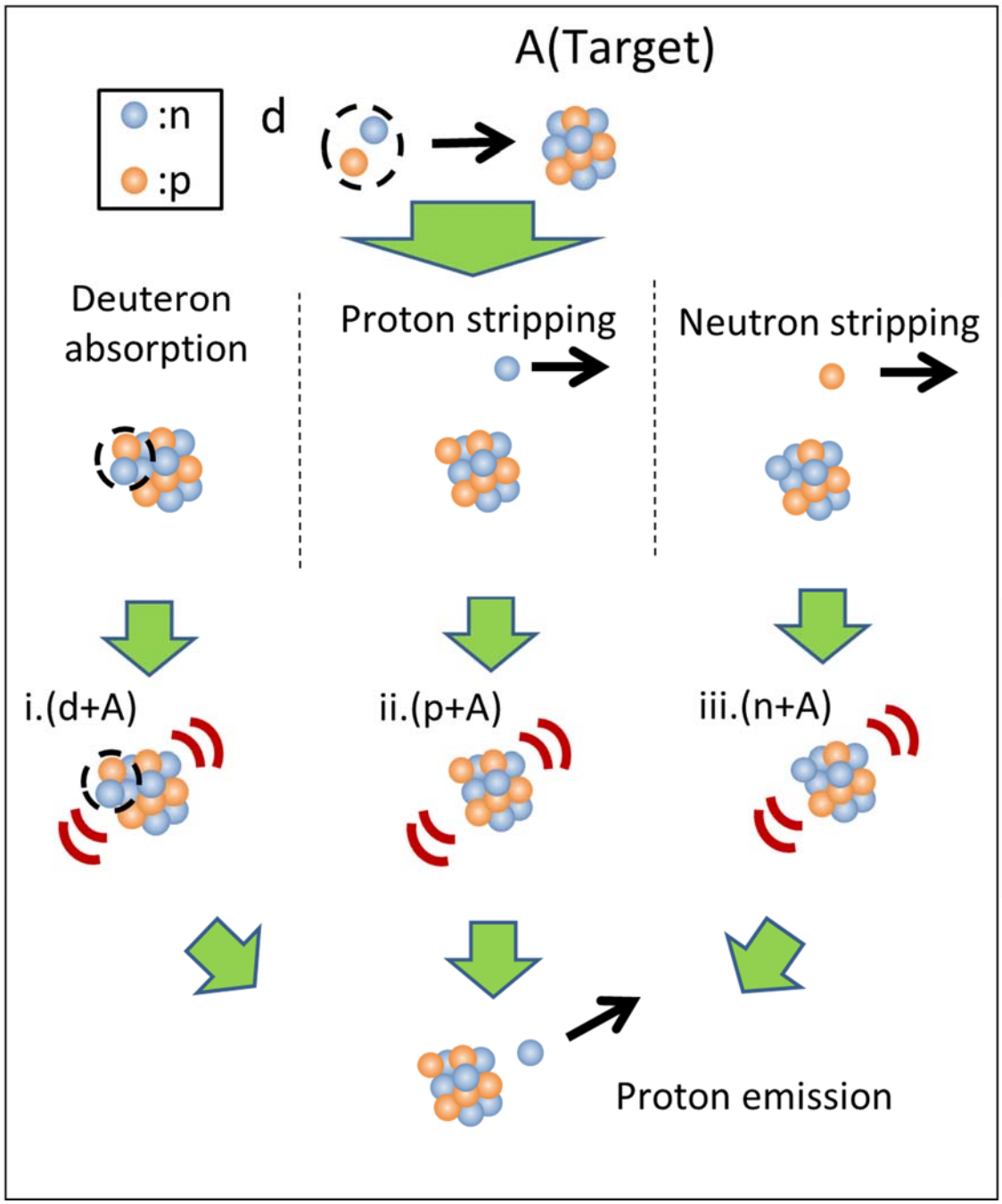

Fig. 4.1 Schematic figure of formation of three different compound nuclei.

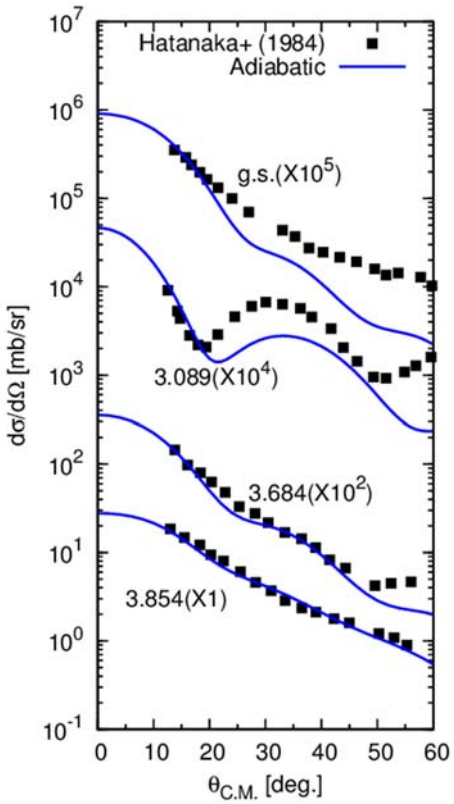

Fig. 4.2 Calculated and experimental differential cross sections for ^{12}C(d,p)^{13}C reactions at E_0 = 56 MeV.

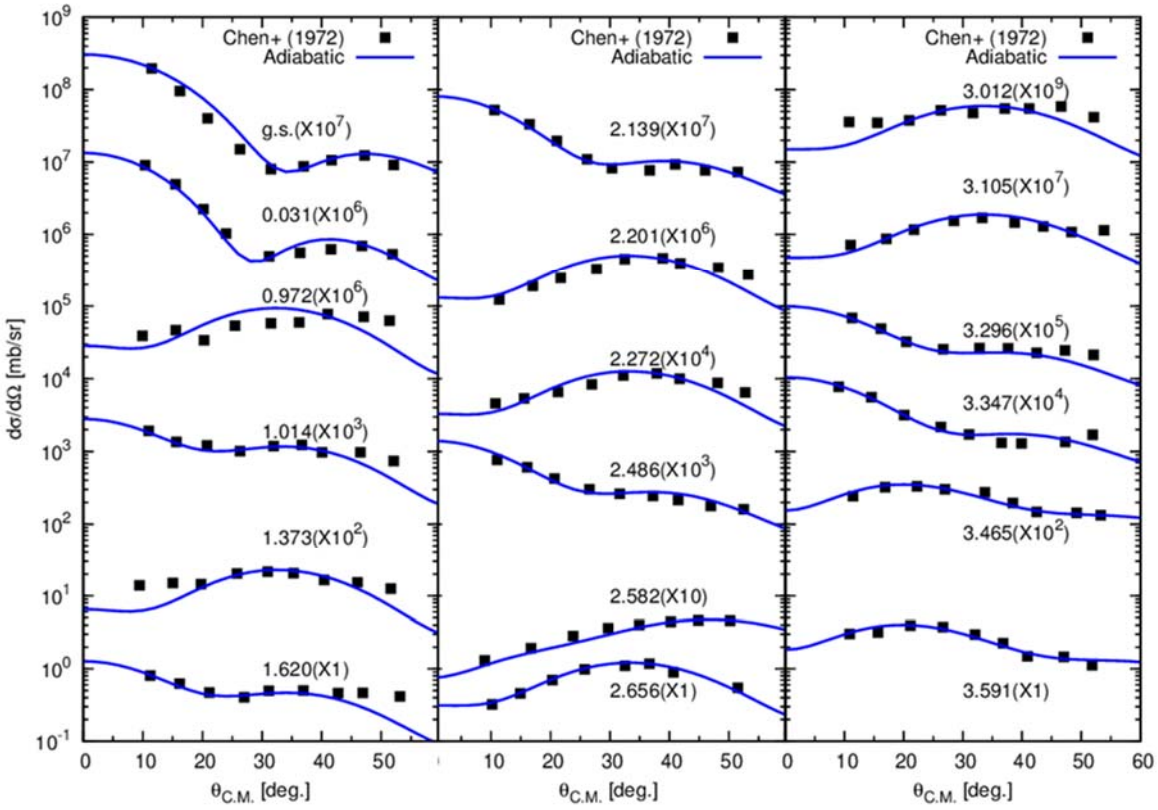

Fig. 4.3 Same as Fig. 4.2 but for ^{27}Al(d,p)^{28}Al reactions at E_0 = 6 MeV.

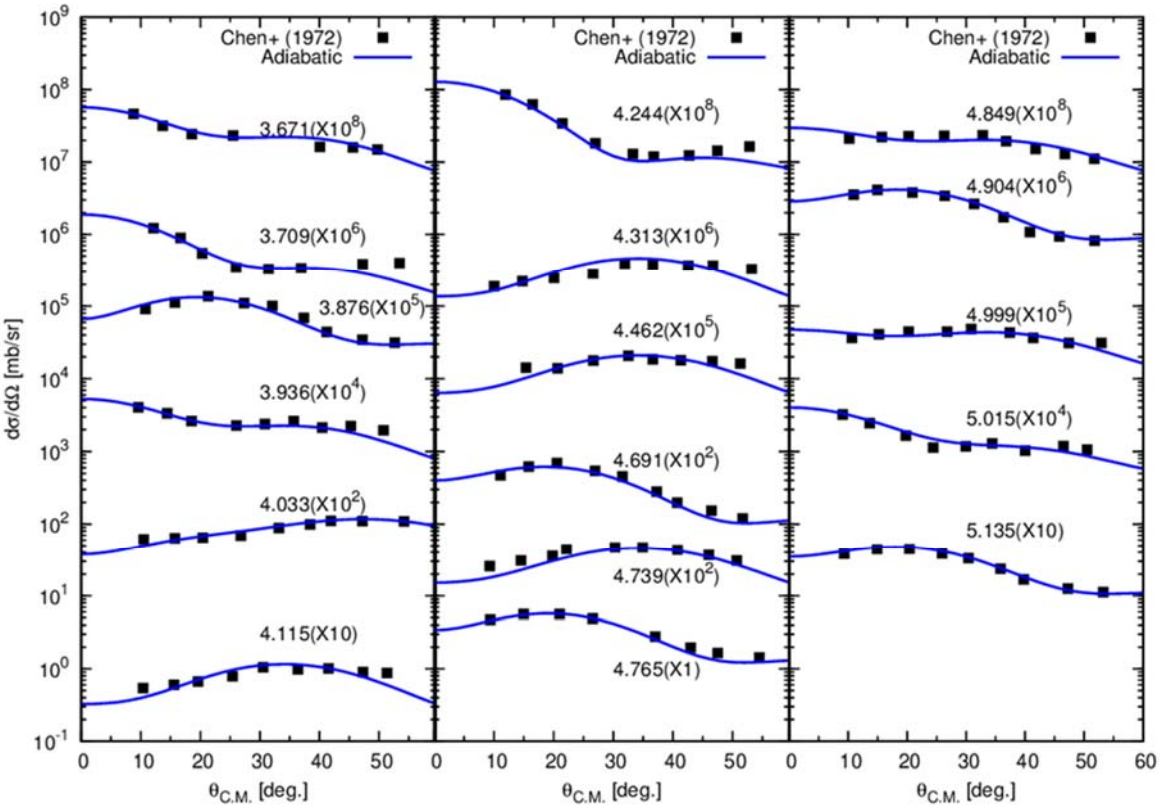

Fig. 4.3 (*Continued.*)

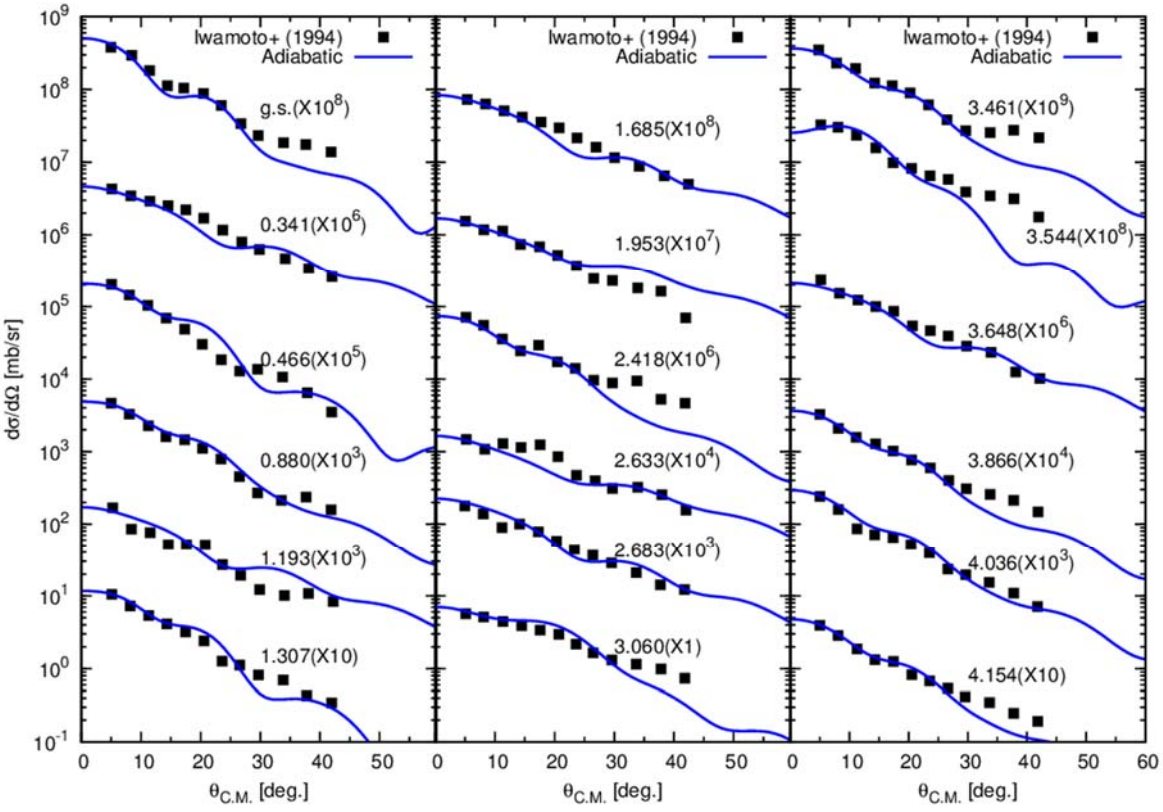

Fig. 4.4 Same as Fig. 4.2 but for ^{58}Ni(d,p)^{59}Ni reactions at E_0 = 56 MeV.

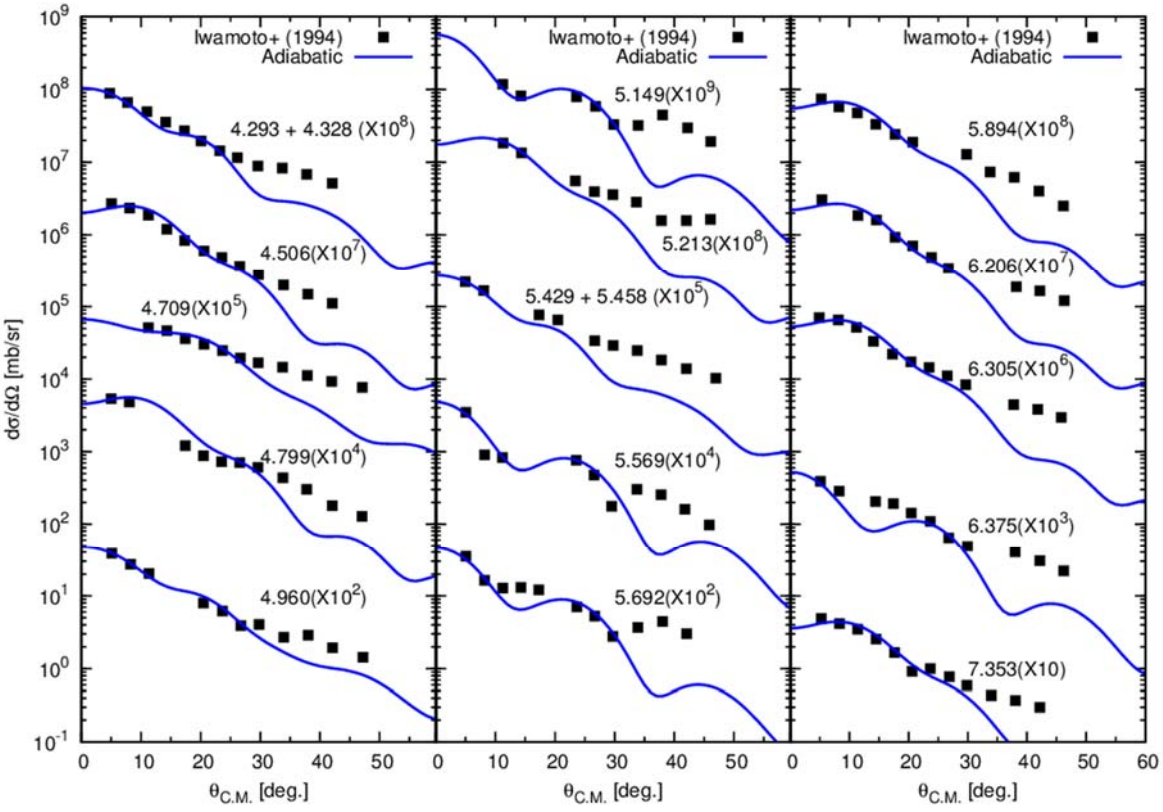

Fig. 4.4 (*Continued.*)

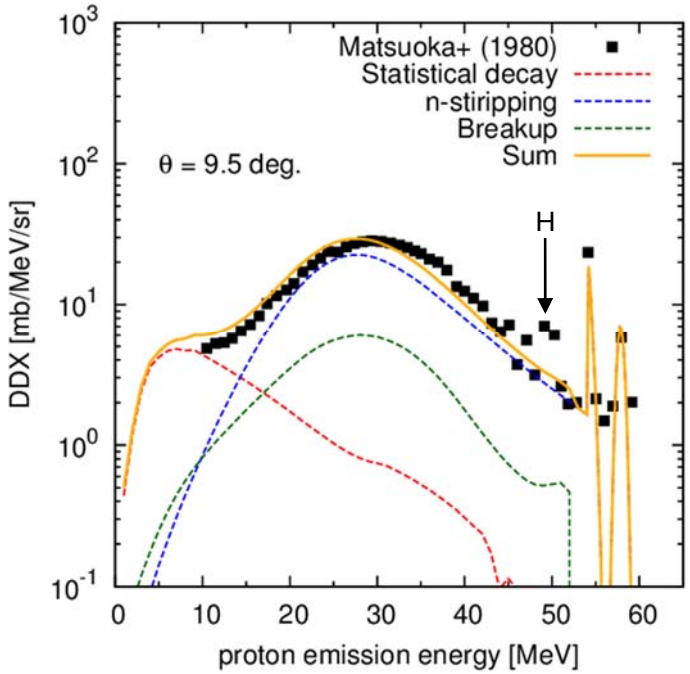

Fig. 4.5 Calculated and experimental double differential cross sections for ^{12}C(*d*,*xp*) reactions at 56 MeV.
"H" denotes the effect of hydrogen contamination.

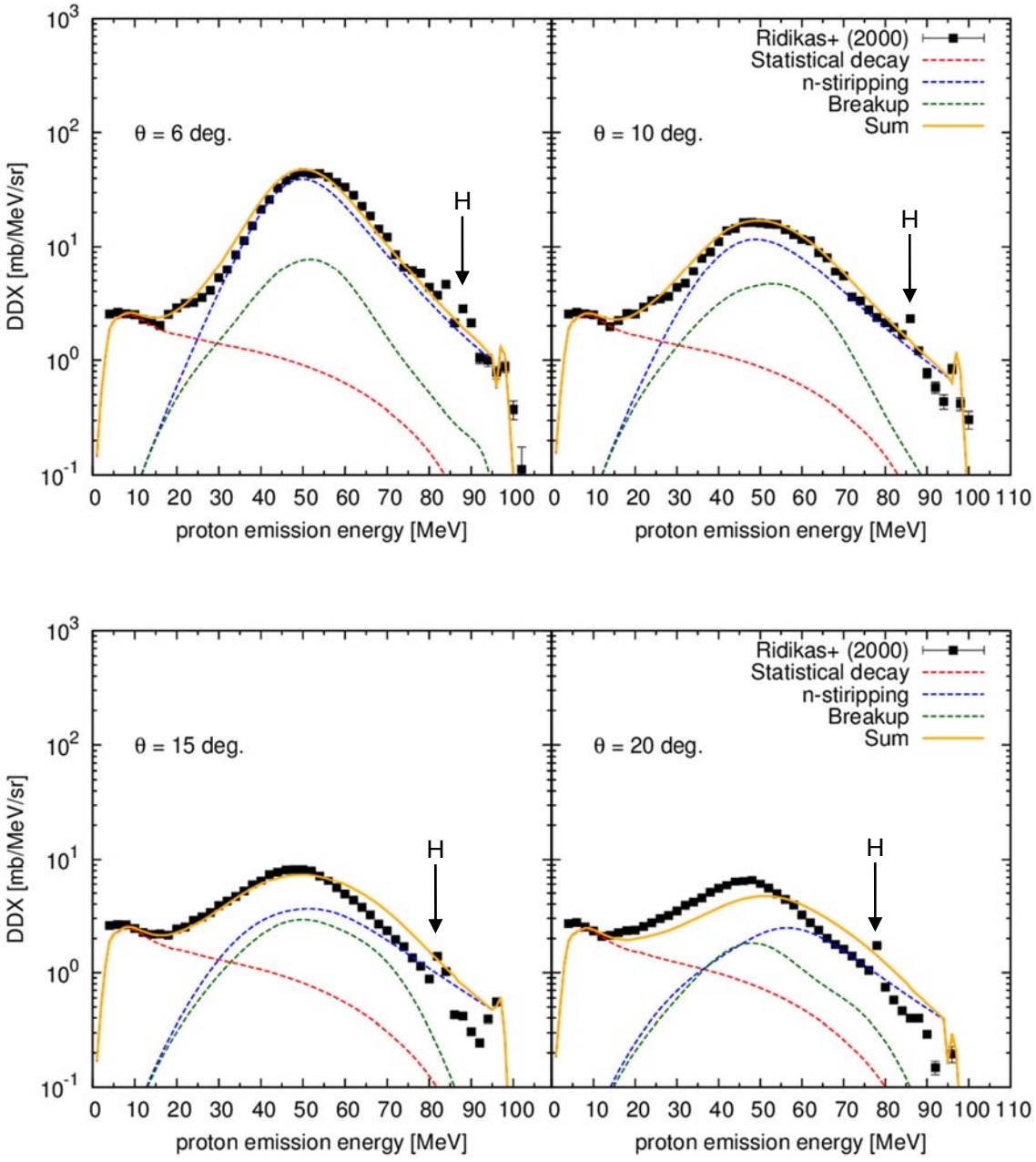

Fig. 4.6 Same as Fig. 4.5 but for ^{12}C(*d*,*xp*) reactions at 100 MeV.

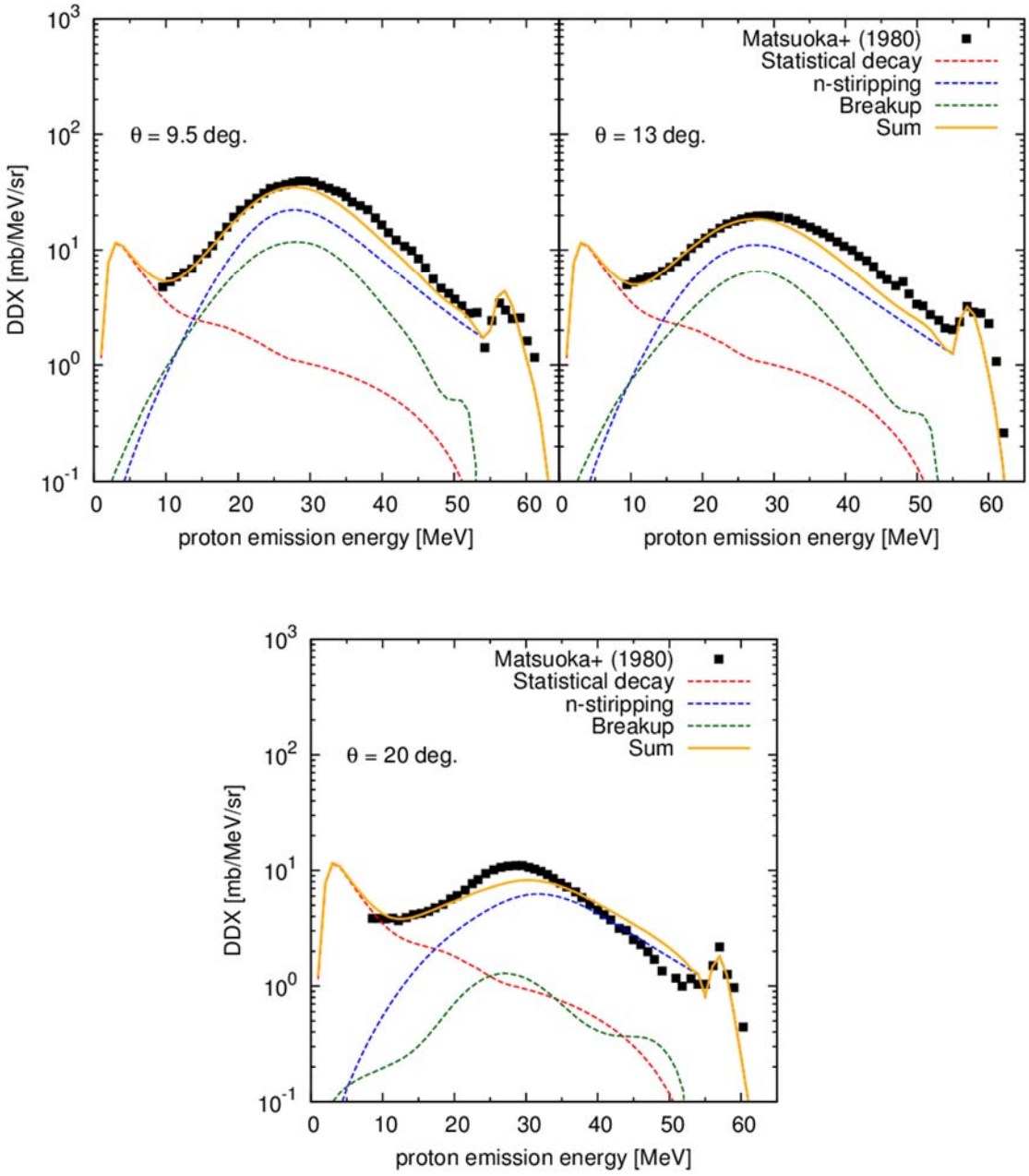

Fig. 4.7 Same as Fig. 4.5 but for ^{27}Al(*d*,*xp*) reactions at 56 MeV.

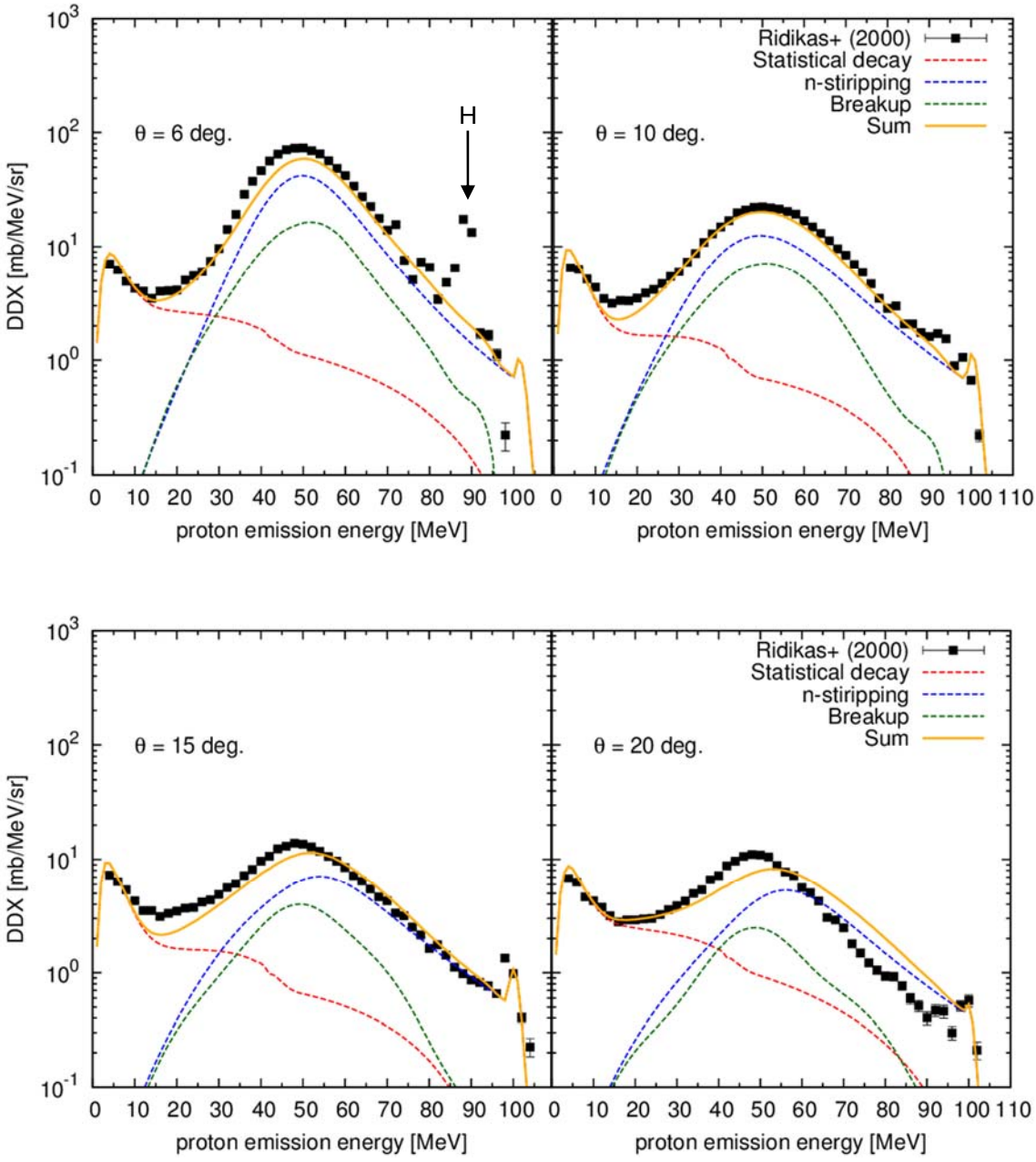

Fig. 4.8 Same as Fig. 4.5 but for ^{27}Al(*d*,*xp*) reactions at 100 MeV.

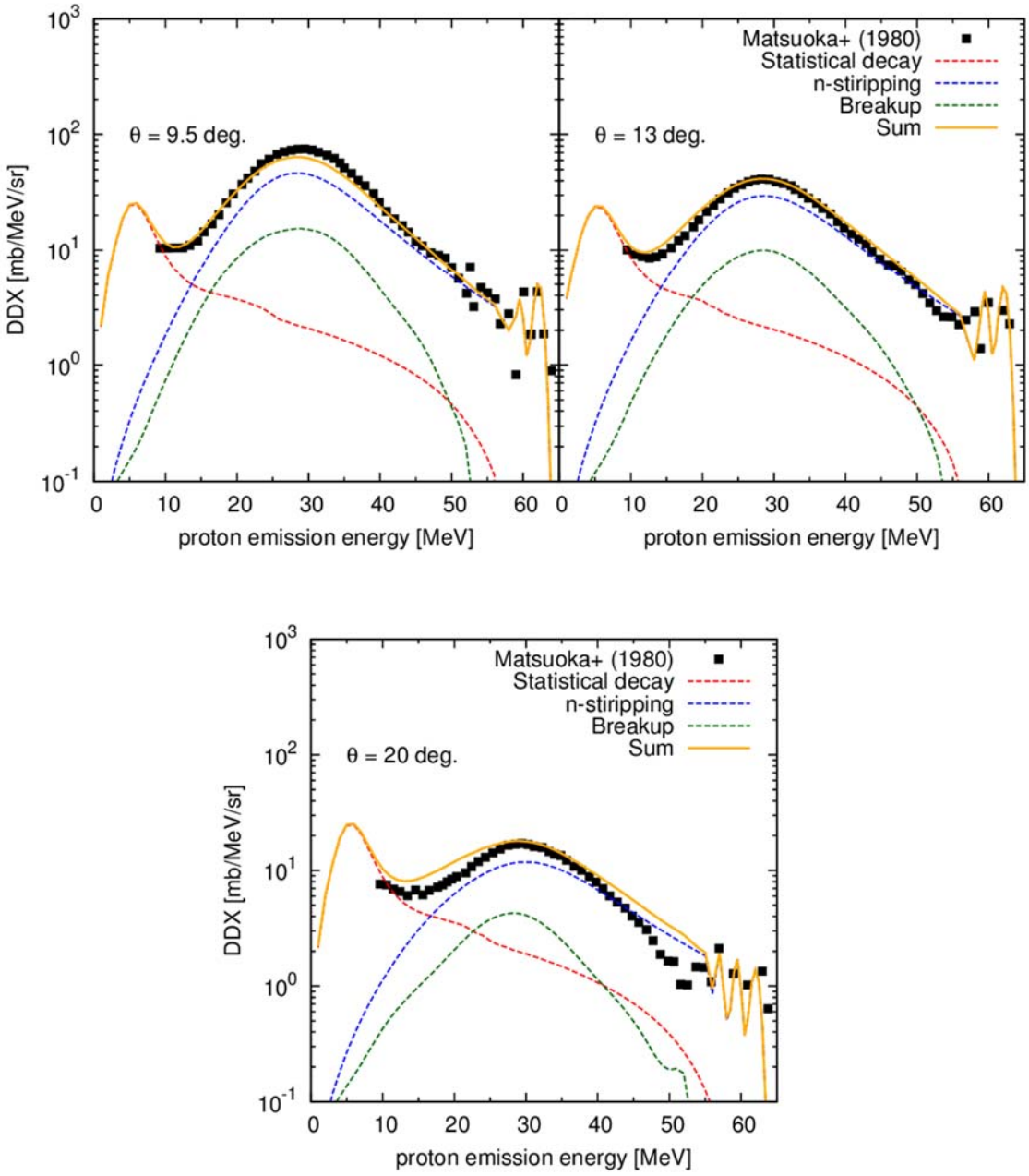

Fig. 4.9 Same as Fig. 4.5 but for ^{58}Ni(*d*,*xp*) reactions at 56 MeV.

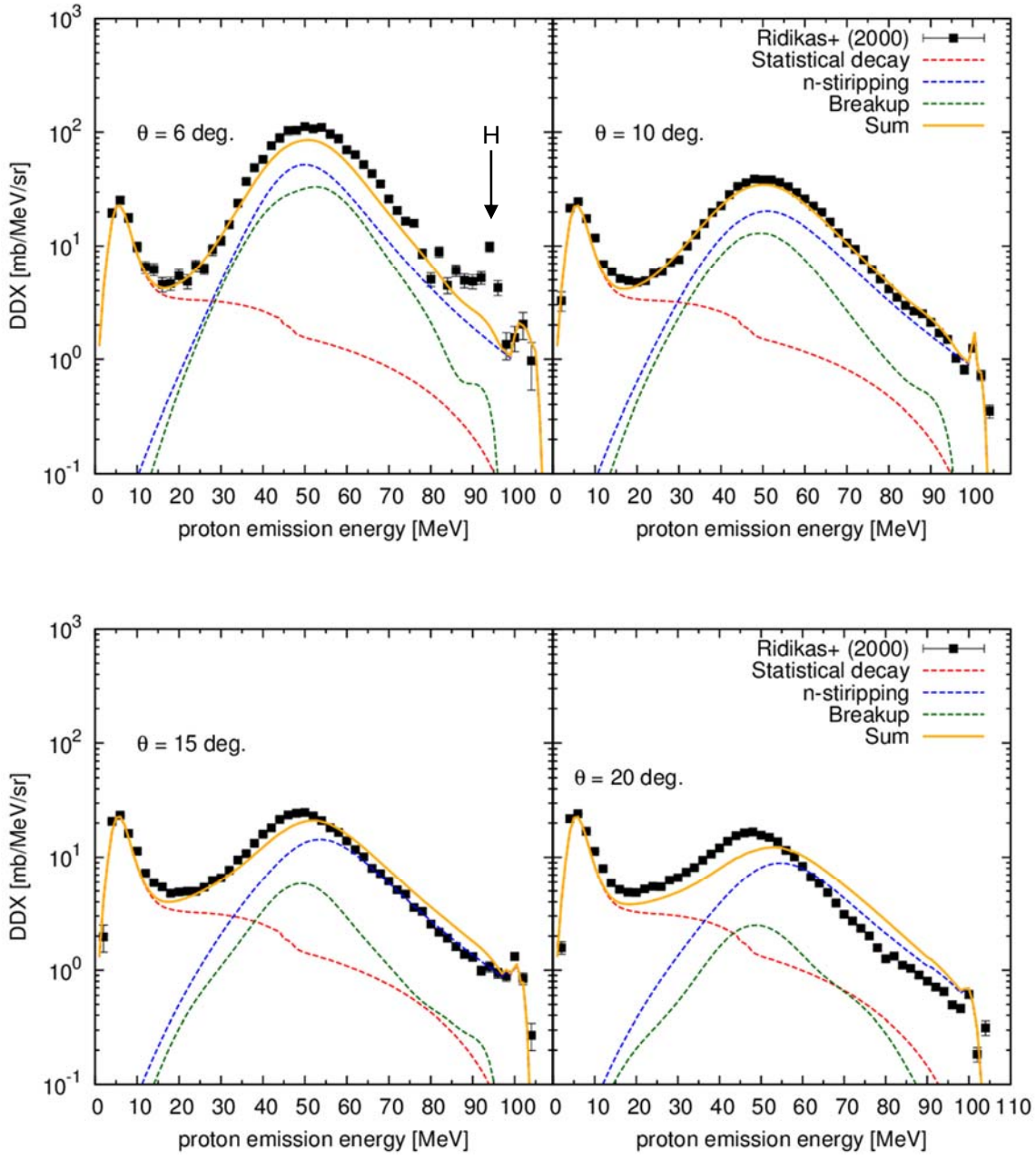

Fig. 4.10 Same as Fig. 4.5 but for ^{58}Ni(*d,xp*) reactions at 100 MeV.

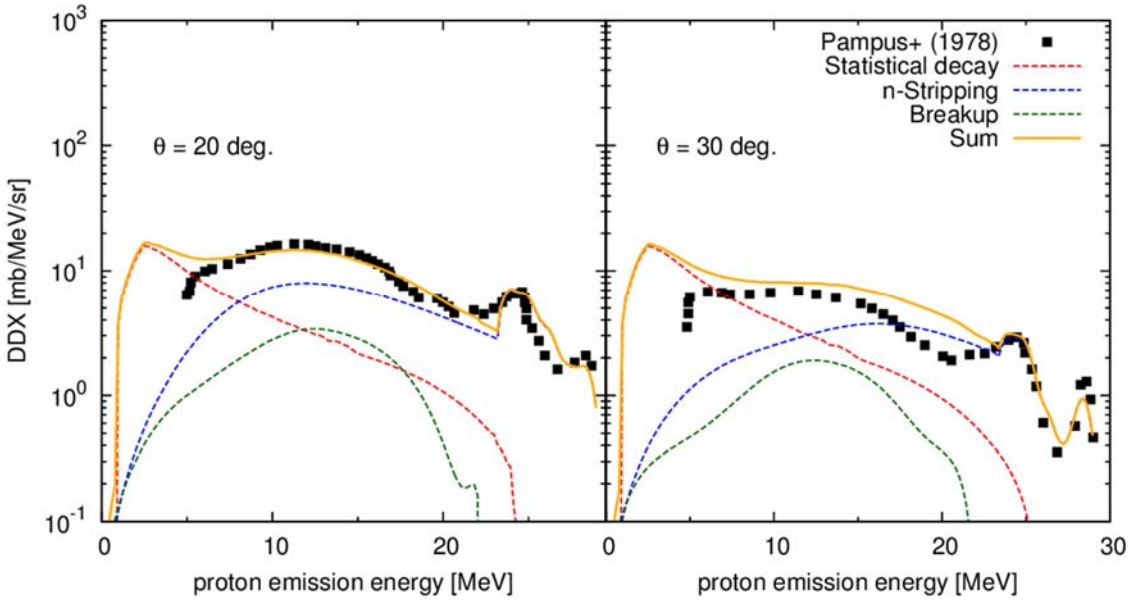

Fig. 4.11 Same as Fig. 4.5 but for ^{27}Al(*d*,*xp*) reactions at 25.5 MeV.

Bibliography

[4.1] M. Yahiro, K. Ogata, T. Matsumoto, K. Minomo, "The continuum discretized coupled-channels method and its applications", Prog. Theor. Exp. Phys. **2012**, 01A206 (2012), and references therein.

[4.2] O. Iwamoto, "Development of a comprehensive code for nuclear data evaluation, CCONE, and validation using neutron-induced cross sections for uranium isotopes", J. Nucl. Sci. Technol. **44**, 687-697 (2007).

[4.3] S. Araki, "Study of statistical decay model in deuteron induced nuclear reactions", Bachelor thesis, Kyushu University, (2012).

[4.4] A. J. Koning, J. P. Delaroche, "Local and global nucleon optical models from 1 keV to 200 MeV", Nucl. Phys. A **713**, 231-310 (2003).

[4.5] H. Hatanaka, N. Matsuoka, T. Saito, K. Hosono, M. Kondo, S. Kato, T. Higo, S. Matsuki, Y. Kaodota, K. Ogino, "Systematic study of the (d, p) reaction with 56 MeV polarized deuterons", Nucl. Phys. A **419**, 530-546 (1984).

[4.6] S. Chen, J. Rapaport, H. Enge, W. W. Buechner, "Level structure of ^{28}Al", Nucl. Phys. A **197**, 97-105 (1972).

[4.7] O. Iwamoto, A. Nohtomi, Y. Uozumi, T. Sakae, M. Matoba, M. Nakano, T. Maki, N. Koori, "Single-particle states in ^{59}Ni with ^{58}Ni(d,p)^{59}Ni reaction at 56 MeV and neutron-bound-state complex potentials", Nucl. Phys. A **576**, 387-408 (1994).

[4.8] D. G. Madland, "Recent results in the development of a global medium-energy nucleon-nucleus optical-model potential", Proc. Specialists' Meeting on Preequilibrium Nuclear Reactions, 103-110, Semmering, Austria, 10-12 Feb (1988).

[4.9] N. Matsuoka, M. Kondo, A. Shimizu, N. Saito, S. Nagamachi, H. Sakaguchi, A. Goto, F. Ohtani, "Deuteron break-up in the field of

nuclei at 56 MeV", Nucl. Phys. A **345**, 1-12 (1980).

[4.10] D. Lidikas, W. Mittig, H. Savajols, P. Roussel-Chomaz, S. V. Fortsch, J. J. Lawrie, G. F. Steyn, "Inclusive proton production cross sections in (*d*,*xp*) reactions induced by 100 MeV deuterons", Phys. Rev. C **63**, 014610 (2000).

[4.11] C. Kalbach, "Systematics of continuum angular distributions: Extensions to higher energies", Phys. Rev. C **37**, 2350-2370 (1988).

[4.12] A.J. Koning, S. Hilaire and M.C. Duijvestijn, "TALYS-1.0", Proc. the International Conference on Nuclear Data for Science and Technology, 211-214, Nice, France, 22-27 Apr (2007).

[4.13] J. Pumpus, J. Bisplinghoff, J. Ernst, T. Mayer-Kuckuk, J. Rao Rama, G. Baur, F. Rosel, D. Trautmann, "Inclusive proton spectra from deuteron break-up: Theory and experiment", Nucl. Phys. A **311**, 141-160 (1978).

Chapter 5

Activation cross sections from (*d*, *p*) reactions

For engineering design of deuteron accelerator neutron sources, it is also important to estimate production of radioactive nuclei. It is well known that for activation induced by (*d*,*p*) reactions, the stripping reactions to bounds states in the residual nuclei play an important role. In this chapter, we therefore apply the present code system to calculation of activation cross sections from (*d*,*p*) reactions on ^{27}Al and ^{45}Sc at incident energies from threshold to 50 MeV.

5.1 Calculation method

For the sake of convenience, the case of ^{27}Al(*d*,*p*)^{28}Al are described as an example in the following explanation. The cross section of ^{45}Sc(*d*,*p*)^{46}Sc can also be calculated by exchanging "Al-28" for "Sc-46" in the equations. In the present code system, the production cross section of ^{28}Al ($T_{1/2}$ = 2.2414 min) from (*d*,*p*) reactions are expressed as follows:

$$\sigma_{\text{Al-28}} = \sigma^{STR}_{\text{Al-28}} + \sigma^{SD}_{\text{Al-28}} \tag{5.1}$$

where $\sigma^{STR}_{\text{Al-28}}$ and $\sigma^{SD}_{\text{Al-28}}$ correspond to the production cross section of ^{28}Al for neutron stripping reaction and statistical decay, respectively.

In the code system, all of the neutron stripping reactions to *i*-th bound state up to I_0 are considered. Thus, neutron stripping reaction components are calculated by summation of angle-integrated DWBA differential cross sections up to I_0 as follows:

$$\sigma^{STR}_{\text{Al–28}} = \sum_{i}^{I_0} \int \frac{d\sigma^{DWBA}_{bound,i}}{d\Omega} d\Omega \tag{5.2}$$

The contribution from statistical decay process is calculated using

the Glauber model [5.1] and CCONE code [5.2]. In general, as shown in Fig. 4.1, three different types of compound nuclei can be formed in the case of deuteron-induced reactions. However, since ^{28}Al is not formed by proton absorption on ^{27}Al, the $\sigma^{SD}_{\mathrm{Al-28}}$ at E_d is given by summation of two components:

$$\sigma^{SD}_{\mathrm{Al-28}} = R_d \sigma^{d}_{\mathrm{Al-28}} + R_n \sigma^{n}_{\mathrm{Al-28}} \tag{5.3}$$

where $\sigma^{d}_{\mathrm{Al-28}}$, and $\sigma^{n}_{\mathrm{Al-28}}$ are production cross sections of ^{28}Al from deuteron and neutron-induced reactions calculated with the CCONE code, respectively; R_d, R_n are the formation fraction calculated by the Glauber model as described in Eq. (4.5).

In the present code system, we use the Glauber model with trajectory modification [5.3] to calculate each formation fraction because the eikonal approximation in the Glauber model gets worse at low incident energies below 20 MeV. In Ref. [5.3], it is found that the Glauber model with trajectory modification reproduces experimental data of total reaction cross sections even at low incident energies. Thus, the trajectory modification has been implemented in the present code system for calculation of integrated cross sections based on Ref. [5.3].

5.2 Input parameters of each calculation

As in the calculation of double-differential cross sections for (*d*,*xp*) reactions, the optical potentials (OPs) used in the CCONE code are the global nucleon OPs of Koning and Delaroche (KD) [5.4] for proton and neutron and the adiabatic OP [5.5] for deuteron. Default values in the CCONE code are used for other physical parameters such as level density parameters.

The input parameters in DWBA calculations are the same as those of “Adiabatic” options given in Table 3.1. Spectroscopic factor (SF) value,

$S_{k,i}(E_d)$ are given by Eqs. (3.2) and (3.3) in which $F_{k,i}$ is determined at E_0 so that $S_{k,i}(E_0)$ is equal to the SF value extracted from DWBA analysis. For ^{27}Al, the extracted SF values for each i-th state at E_0 are previously listed in Table 4.2.

For ^{45}Sc, E_0 = 12 MeV [5.6] and I_0 = 140. The extracted SF values and the results of DWBA analysis for ^{45}Sc are shown in Table 5.1 and Fig. 5.1, respectively. It should be noted in Ref. [5.6] angular distribution of (d,p) reaction are shown for the 32 final states and only the maximum values of (d,p) differential cross sections $(d\sigma/d\Omega)_{\max}$ are given for the other 108 states. Therefore, we extract the SF values for these 108 states by fitting the calculated DWBA cross section to experimental data only at the one angle where $(d\sigma/d\Omega)_{\max}$ is given.

5.3 Calculation results and discussion

Figure 5.2 shows the comparison between the calculated and experimental production cross sections of ^{28}Al from ^{27}Al(d,p) reactions. The experimental data are taken from Ref. [5.7]. The sum of the statistical decay components $\sigma^{SD}_{\mathrm{Al-28}}$ and the contribution from neutron stripping to bound states $\sigma^{STR}_{\mathrm{Al-28}}$ reproduce the experimental data in the incident energy region below 20 MeV fairly well. Next, in Fig. 5.3, the calculation results of production cross sections of ^{46}Sc from ^{45}Sc(d,p) reactions are compared with the experimental data [5.8, 5.9]. As in the case of Fig. 5.2, the sum of the statistical decay components and the neutron stripping components reproduce the experimental data fairly well in the wide range of incident energy up to 50 MeV.

As shown in Figs. 5.2 and 5.3, the components of stripping

reactions to bounds states in the residual nuclei have a large contribution in calculation of the activation cross sections from (*d*,*p*) reactions. These components are not considered in TALYS code [5.10], while they are calculated with DWBA approach using derived SF values in the present code system.

Let us discuss the importance of SF values. Figs. 5.4 and 5.5 show the comparisons of calculation results using the different SF values. In "An-Cai SF" cases, the SF values extracted from "An-Cai" option DWBA analysis are used and the calculation results overestimate the experimental data. From these results, we can conclude that it is not appropriate to use the SF values derived from different analysis conditions. As in this work, we should extract the SF values directly from experimental data instead of using the SF values cited in the literatures if the conditions in DWBA calculations, such as OPs, are different.

The results of Fig. 5.2 to 5.5 demonstrate that it is of importance to consider the stripping reaction to bound states appropriately, especially in the evaluation of deuteron-induced radioactivity.

5.4 Summary

The present code system was applied to analysis of production cross section of radioactive nuclei from (*d*,*p*) reactions. As a result of the analysis, the calculation using the code system reproduced the measured activation cross sections from (*d*,*p*) reactions on ^{27}Al and ^{45}Sc at incident energies from threshold to 50 MeV fairly well. The results confirm that the reaction models used in the present calculations are also valid for production cross section of residual nuclei from (*d*,*p*) reactions.

Table 5.1 List of spectroscopic factors for ^{45}Sc(d,p)^{46}Sc reactions extracted from the present analysis at E_0 = 12 MeV.

i	E_{ex} [MeV]	J_i^π	l	$S_{\text{Sc-45},i}$	i	E_{ex} [MeV]	J_i^π	l	$S_{\text{Sc-45},i}$
1	0(g.s.)	4^+	3	0.46	19	1.770	$(2,3,4)^+$	1	0.09*
2	0.049	6^+	3	0.76	20	1.804	$(2,3)^+$	1	0.52*
3	0.227	3^+	3	0.60	21	1.852	1^+	1	0.01
4	0.280	5^+	1, 3	0.04, 0.04	22	1.885	3^+	3	0.13
5	0.446	2^+	3	0.38	23	2.073	3^+	1	0.13
6	0.773	5^+	3	0.31	24	2.117	3^+	1	0.14
7	0.835	4^+	3	0.30	25	2.210	-	3	0.19*
8	0.978	7^+	3	0.28	26	2.225	2^+	1	0.06
9	1.006	1^+	3	0.31	27	2.307	$(2,3,4)^+$	1	0.26*
10	1.092	4^+	1	0.02	28	2.332	-	1	4.63*
11	1.131	4^+	0	0.003	29	2.371	-	1	0.09*
12	1.142	-	0	0.03*	30	2.415	3^+	1	0.11
13	1.325	3^+	3	0.08	31	2.455	3^+	1	0.20
14	1.397	2^+	1	0.01	32	2.534	4^+	1	0.07
15	1.438	-	0	0.01*	33	2.565	$(3,4)^+$	1	1.06*
16	1.648	4^-	0	0.01	34	2.592	$(3,4)^+$	2	0.22*
17	1.676	-	1	0.30*	35	2.650	$(2,3,4)^+$	2	0.17*
18	1.753	-	3	0.75*	36	2.672	3^+	1	0.01

* The value of $(2J_i+1)S_i$ is presented since J_i is not assigned.

Table 5.1 (*Continued.*)

i	E_{ex} [MeV]	J_i^π	l	$S_{\text{Sc-45},i}$	i	E_{ex} [MeV]	J_i^π	l	$S_{\text{Sc-45},i}$
37	2.714	2^+	1	0.35	55	3.450	$(2,3,4)^+$	1	0.58*
38	2.760	-	1	0.06*	56	3.481	$(2,3,4)^+$	1	0.57*
39	2.785	$(3,4)^-$	0	0.14*	57	3.512	-	1	0.55
40	2.815	1^+	1	0.14	58	3.538	$(2,3,4)^+$	1	0.58*
41	2.841	$(2,3,4)^+$	1	0.06*	59	3.615	$(3,4,5)^+$	1	0.87*
42	2.863	2^+	1	0.38	60	3.661	4^+	1	0.02
43	2.898	-	1	0.24*	61	3.696	$(2,3,4)^+$	1	0.21*
44	2.942	-	0	0.06*	62	3.722	-	1	0.05*
45	2.980	$(3,4)^+$	1	1.23*	63	3.770	3^+	1	0.13
46	3.033	-	1	0.58*	64	3.790	4^+	1	0.02
47	3.063	-	1	0.88*	65	3.818	-	1	0.25*
48	3.090	$(2,3,4)^+$	1	0.54*	66	3.837	$(3,4)^+$	1	0.05*
49	3.143	$(3,4)^-$	0	0.03*	67	3.877	$(3,4)^+$	1	0.35*
50	3.184	4^+	1	0.16	68	3.936	-	1	0.16*
51	3.243	$(0,1)^+$	1	1.21*	69	3.961	-	1	0.04*
52	3.323	-	1	0.32*	70	3.983	-	1	0.06*
53	3.394	$(2,3,4)^+$	1	0.91*	71	4.008	-	1	0.21*
54	3.422	3^+	1	0.13	72	4.029	-	1	0.07*

* The value of $(2J_i+1)S_i$ is presented since J_i is not assigned.

Table 5.1 (*Continued.*)

i	E_{ex} [MeV]	J_i^{π}	l	$S_{\text{Sc-45},i}$	i	E_{ex} [MeV]	J_i^{π}	l	$S_{\text{Sc-45},i}$
73	4.068	-	1	0.06*	91	4.846	-	1	1.19*
74	4.088	-	1	0.74*	92	4.896	-	1	0.70*
75	4.153	$(0,1)^-$	2	0.78*	93	4.927	-	2	1.14*
76	4.229	-	3	1.37*	94	4.956	-	1	0.42*
77	4.288	-	1	0.15*	95	5.010	-	1	0.49*
78	4.311	-	1	0.14*	96	5.045	-	1	0.21*
79	4.350	-	3	0.25*	97	5.075	-	1, 3	0.33*, 5.89*
80	4.381	-	1	1.01*	98	5.113	-	1	0.55*
81	4.470	-	1	0.58*	99	5.149	-	0	0.18*
82	4.498	-	1	0.53*	100	5.165	-	1	0.63*
83	4.518	-	1	0.46*	101	5.192	-	1	0.99*
84	4.575	-	1	0.20*	102	5.250	-	3	0.50*
85	4.616	-	1	0.47*	103	5.344	-	0	0.13*
86	4.649	-	1	0.10*	104	5.404	-	1	0.93*
87	4.666	-	1	0.30*	105	5.427	-	1	0.63*
88	4.689	-	1	0.59*	106	5.445	-	1	0.16*
89	4.755	-	1	0.69*	107	5.491	-	3	0.39*
90	4.794	-	0	0.10*	108	5.514	-	1	0.41*

* The value of $(2J_i + 1)S_i$ is presented since J_i is not assigned.

Table 5.1 (*Continued.*)

i	E_{ex} [MeV]	J_i^{π}	l	$S_{\text{Sc-45},i}$
109	5.563	-	0	0.14*
110	5.595	-	1	0.41*
111	5.620	-	1	0.32*
112	5.659	-	1	0.67*
113	5.753	-	3	0.67*
114	5.772	-	1	0.11*
115	5.814	-	1	0.20*
116	5.837	-	1	0.23*
117	5.878	-	1	0.13*
118	5.928	-	1	0.15*
119	5.979	-	1	0.08*
120	6.004	-	1	0.21*
121	6.037	-	1, 3	0.08*, 2.1*
122	6.061	-	1	0.13*
123	6.083	-	1	0.12*
124	6.110	-	1	0.10*
125	6.145	-	1	0.15*
126	6.159	-	1	0.22*
127	6.191	-	3	3.00*
128	6.276	-	1	0.17*
129	6.295	-	3	1.41*
130	6.362	-	1	0.07*
131	6.380	-	1	0.04*
132	6.405	-	3	1.74*
133	6.429	-	1	0.17*
134	6.454	-	1	0.06*
135	6.469	-	1	0.12*
136	6.497	-	1	0.04*
137	6.525	-	1	0.06*
138	6.549	-	1	0.11*
139	6.612	-	1	0.15*
140	6.650	-	1	0.13*

* The value of $(2J_i + 1)S_i$ is presented since J_i is not assigned.

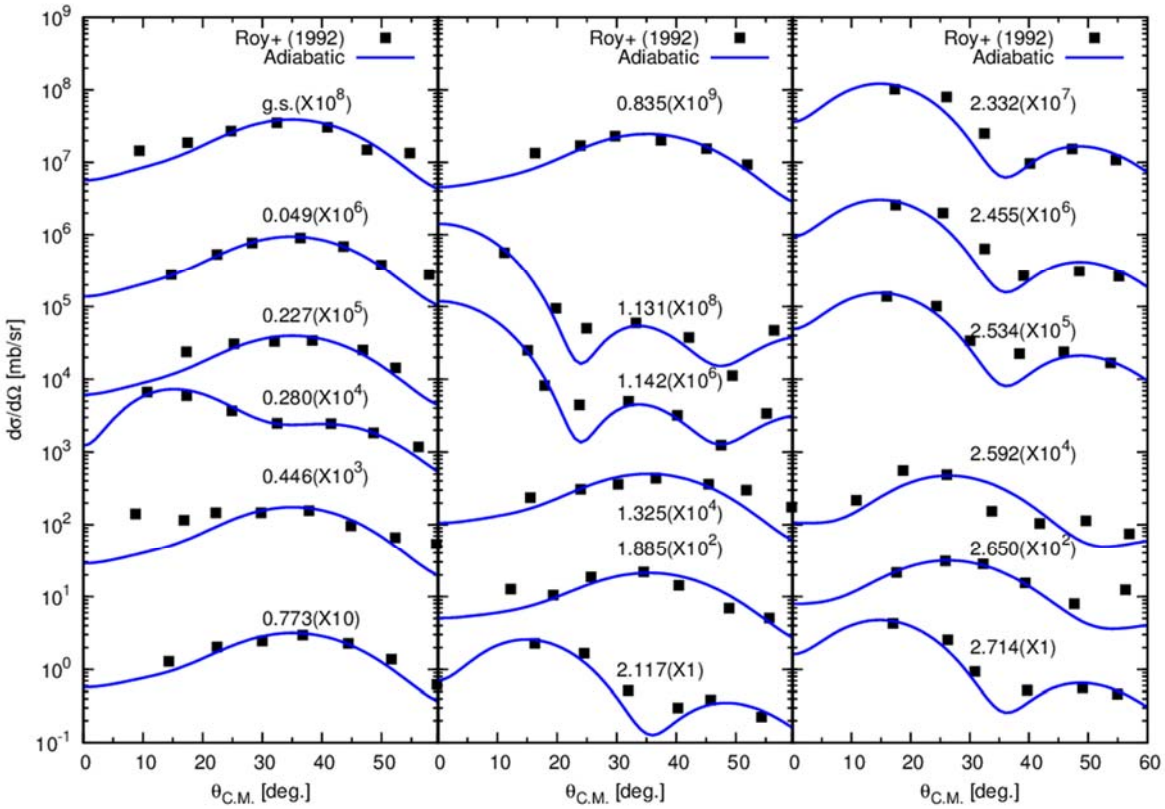

Fig. 5.1 Calculated and experimental differential cross sections for ^{45}Sc(d,p)^{46}Sc reactions at E_0 = 12 MeV.

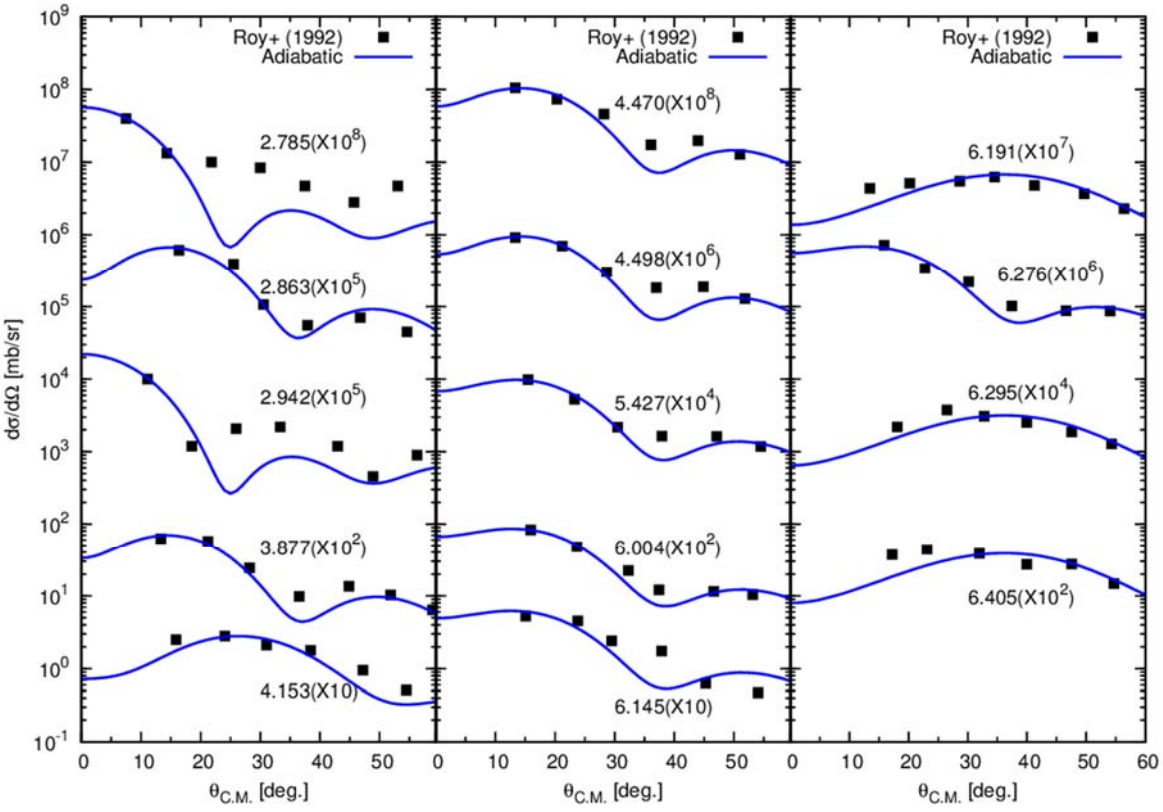

Fig. 5.1 (*Continued.*)

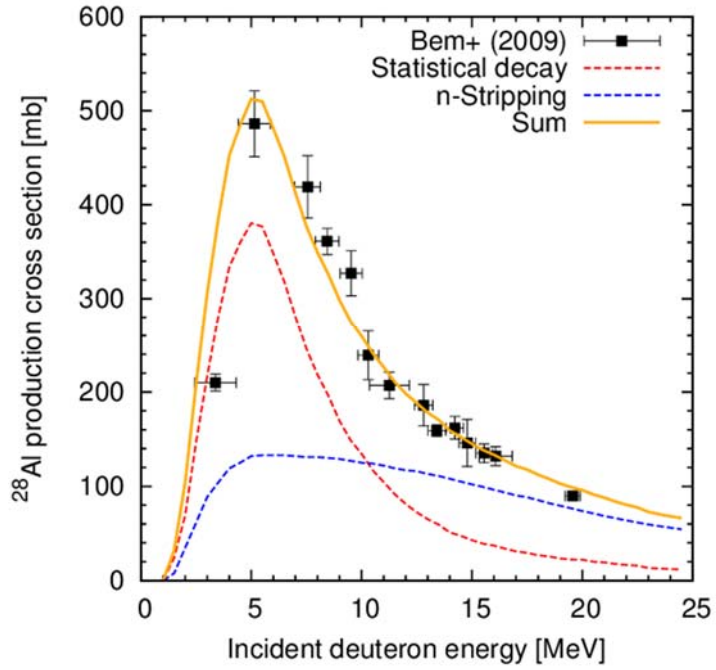

Fig. 5.2 Production cross sections of ^{28}Al from ^{27}Al(d,p) reactions.

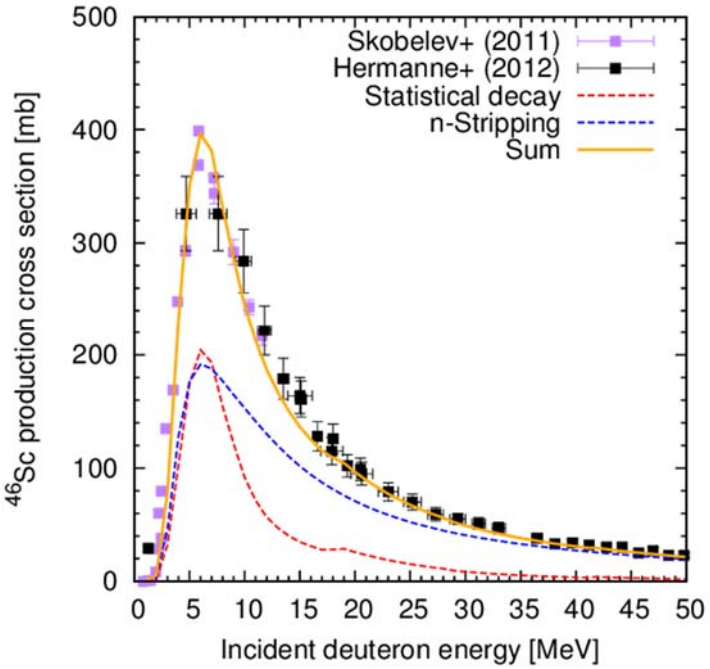

Fig. 5.3 Production cross sections of ^{46}Sc from ^{45}Sc(d,p) reactions.

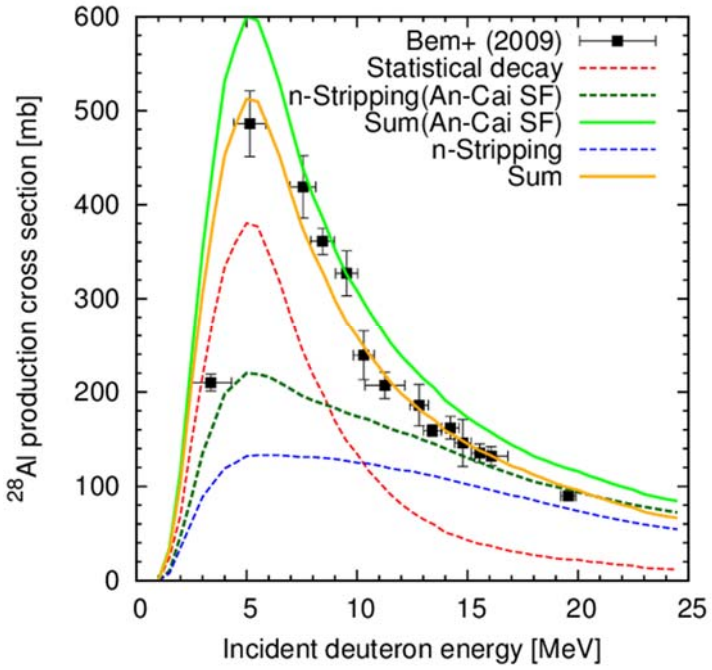

Fig. 5.4 Production cross sections of ^{28}Al from ^{27}Al(d,p) reactions using SF values extracted from "An-Cai" option.

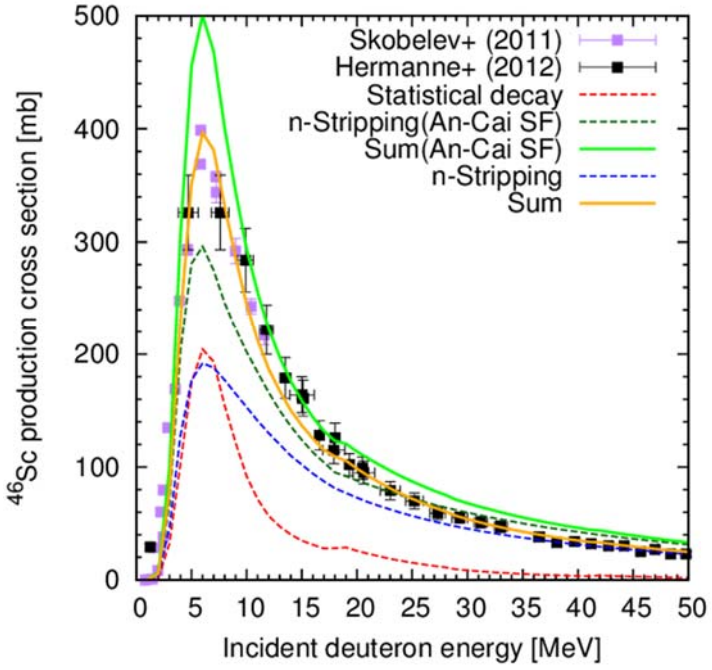

Fig. 5.5 Production cross sections of ^{46}Sc from ^{45}Sc(d,p) reactions using SF values extracted from "An-Cai" option.

Bibliography

[5.1] T. Ye, S. Hashimoto, Y. Watanabe, K. Ogata, M. Yahiro, "Analysis of inclusive (*d*,*xp*) reactions on nuclei from ^{9}Be to ^{238}U at 100 MeV", Phys. Rev. C **84**, 054606 (2011).

[5.2] O. Iwamoto, "Development of a comprehensive code for nuclear data evaluation, CCONE, and validation using neutron-induced cross sections for uranium isotopes", J. Nucl. Sci. Technol. **44**, 687-697 (2007).

[5.3] T. Ye, Y. Watanabe, "Systematic study of deuteron-induced reactions from threshold", Nucl. Data Sheets **118**, 308-311 (2014).

[5.4] A. J. Koning, J. P. Delaroche, "Local and global nucleon optical models from 1 keV to 200 MeV", Nucl. Phys. A **713**, 231-310 (2003).

[5.5] D. G. Madland, "Recent results in the development of a global medium-energy nucleon-nucleus optical-model potential", Proc. Specialists' Meeting on Preequilibrium Nuclear Reactions, 103-110, Semmering, Austria, 10-12 Feb (1988).

[5.6] J. N. Roy, A. R. Majumder, H. M. Sen Gupta, "^{45}Sc(*d*,*p*)^{46}Sc reaction", Phys. Rev. C **46**, 144-157 (1992).

[5.7] P. Bem, E. Simeckova, M. Honusek, U. Fischer, S. P. Simakov, R. A. Forrest, M. Avrigeanu, A. C. Obreja, F. L. Roman, V. Avrigeanu, "Low and medium energy deuteron-induced reactions on ^{27}Al", Phys. Rev. C **79**, 044610 (2009).

[5.8] A. Hermanne, R. Adam Rebeles, F. Tarkanyi, S. Takacs, M.P. Takacs, J. Csikai, A. Ignatyuk, "Cross sections of deuteron induced reactions on ^{45}Sc up to 50 MeV: Experiments and comparison with theoretical codes", Nucl. Inst. Meth. B **270**, 106-115 (2012).

[5.9] N.K. Skobelev, A.A. Kulko, V. Kroha, V. Burjan, Z. Hons, A.V. Daniel, N.A. Demekhina, R. Kalpakchieva, A. Kugler, J. Mrazek,

Yu.E. Penionzhkevich, S. Piskor, E. Simeckova, E.I. Voskoboynik, “Excitation functions for the radionuclide ^{46}Sc produced in the irradiation of ^{45}Sc with Deuterons and ^{6}He, J. Phys. G Nucl. Part. Phys. **38** 035106 (2011).

[5.10] A.J. Koning, S. Hilaire and M.C. Duijvestijn, “TALYS-1.0”, Proc. the International Conference on Nuclear Data for Science and Technology, 211-214, Nice, France, 22-27 Apr (2007)

Chapter 6

Summary and future works

6.1 Summary of this work

In recent years, intensive neutron sources using deuteron accelerator have been proposed for various neutron beam applications such as irradiation testing of fusion reactor materials, production of radioisotopes for medical use, and so on. For development and detailed design of such accelerator-driven neutron sources, accurate and comprehensive nuclear data of deuteron-induced reactions are indispensable as fundamental data. Currently, available deuteron nuclear data can be found in TENDL (TALYS-based evaluated nuclear data library), which has been developed by compiling the output of the TALYS code. However, TALYS code is not necessarily adequate for calculation of deuteron-induced reactions. Under these situations, we have started to develop a reliable calculation method for deuteron-induced reactions and an integrated code system based on it for development of new deuteron nuclear data.

In Chapter 2, brief explanations about the integrated code system we developed and the theoretical models used in it were provided. In the code system, elastic breakup and stripping reactions to continuum are calculated using the codes based on the Continuum-Discretized Coupled-Channels theory (CDCC) and the Glauber model, respectively. In addition, the DWUCK4, which is the computational code based on a conventional zero-range distorted wave Born approximation (DWBA) is used to calculate stripping reaction to bound states in the residual nuclei. Finally, statistical decay component from compound nuclei are calculated using the Hauser-Feshbach and exciton models implemented in CCONE code.

In Chapter 3, systematic investigation of spectroscopic factor (SF)

which is necessary to determine the absolute values of DWBA calculations were performed. SFs for the (d,p) reactions on ^{12}C, ^{27}Al, ^{40}Ca, and ^{58}Ni for incident deuteron energies up to 100 MeV were extracted systematically by fitting theoretical DWBA calculations to the exiting experimental data. As the results of the DWBA analysis, it was shown that the absolute value of SF depends strongly on deuteron optical potentials used in DWBA calculation. In addition, the extracted SFs showed similar incident energy dependence among all the target nuclei. Finally, an empirical expression describing the energy dependence was deduced.

In Chapter 4, the present code system was applied to analysis of double-differential cross sections (DDXs) for (d,xp) reactions. As the result of analysis, the calculation using the code system reproduced measured DDXs for (d,xp) reactions on ^{12}C, ^{27}Al, and ^{58}Ni at 25.5, 56, and 100MeV fairly well.

In Chapter 5, the present code system was also applied to analysis of production cross section of radioactive nuclei from (d,p) reactions. As the result of analysis, the calculation using the code system reproduced measured production cross sections of ^{28}Al and ^{46}Sc at incident energies from threshold to 50 MeV fairly well.

The results of Chapters 4 and 5 demonstrate the applicability of the code system to the proton emission reaction induced by deuteron.

6.2 Future works

In this work, the code system we developed for the proton emission reaction induced by deuteron was validated. In addition, it was found that the neutron SFs extracted from the present DWBA analysis show similar incident energy dependence regardless of the target nucleus. For deuteron nuclear data evaluation, scaling factor $F_{k,i}$, which determine the absolute value of SF should be obtained corresponding to the various target nuclei k and their excited states i. Therefore, we need to establish a theoretical or phenomenological method to describe $F_{k,i}$ comprehensively.

Further analysis will be necessary for other quantities such as DDXs of (*d,xn*) reactions. Since available experimental DDXs of (*d,xn*) data are very limited, however, the analysis of measured thick target neutron yields (TTYs) would be useful for validation of the code system. Systematic analysis of TTY data will also be favorable from the other point of view. Available experimental data of differential cross section of (*d*,*n*) reactions are also limited. Therefore, it is difficult to extract proton SFs and to investigate its energy dependence. If experimental (*d*,*n*) data are not enough, we cannot help assuming the same energy dependence of proton SFs for (*d*,*n*) reactions as that of neutron SFs extracted in the present work. In such the cases, analysis of TTYs data will be useful for validation of energy dependence of SFs because neutron emission spectra at energies from incident deuteron energy to zero are required in the calculation of TTYs.

Acknowledgements

This work carried out at the Department of Advanced Energy Engineering Science, Interdisciplinary Graduate School of Engineering Sciences, Kyushu University, under the supervision of Professor Yukinobu Watanabe. This dissertation would not have been accomplished without the support of many people and I would like to express my sincere thanks to all of them.

First of all, I would like to thank my supervisor, Professor Yukinobu Watanabe, with my deepest gratitude. His direction, comments and encouragements are of great value to me. His comments with deep understanding of nuclear physics and technology gave me a lot of things.

My great thanks are also expressed to Professors Satoshi Fukada and Masanobu Yahiro for careful reading of this manuscript and valuable comments.

I would like to express my great thanks to Associate Professor Kazuyuki Ogata, Assistant Professor Takuma Matsumoto, and Dr. Shintaro Hashimoto for their fruitful discussion and comments on DWBA analyses. I express further thanks to Associate Professor Kazuyuki Ogata for his suggestions, comments and helpful discussions on CDCC and computational codes.

I also wish to thank very much Dr. Osamu Iwamoto for his help on CCONE code and Dr. Tao Ye for his help on computational code based on the Glaber model.

Furthermore, I would like to thank Assistant Professor Tadahiro Kin and all other members in the Watanabe laboratory for their warmhearted helps. Especially, Mr. Shouhei Araki helped me in various

situation. My thanks are also given to Ms. Megumi Ogami for her help about office work.

This work was supported by Grant-in-Aid for The Japan Society for the Promotion of Science Fellows Grant Number 26・1995. Many thanks are presented to the Japan Society for the Promotion of Science, Kyushu University, and Japan Atomic Energy Agency for their scientific and financial support.

Finally, I would like to thank my parents. Without their supports, I could not finish this work.